1.E.5:
2.A.1

Nuclear Physics A209 (1973) 1—51; © *North-Holland Publishing Co., Amsterdam*

PION REACTION CROSS SECTIONS AND NUCLEAR SIZES

B. W. ALLARDYCE, C. J. BATTY, D. J. BAUGH, E. FRIEDMAN †, G. HEYMANN ††
Rutherford High Energy Laboratory, Chilton, UK

M. E. CAGE ‡, G. J. PYLE, G. T. A. SQUIER
Physics Department, University of Birmingham, UK

A. S. CLOUGH, D. F. JACKSON, S. MURUGESU, V. RAJARATNAM ‡‡
Physics Department, University of Surrey, UK

Received 22 March 1973

Abstract: Measurements have been made of the reaction cross sections of π^- and π^+ mesons for the nuclei C, Ca, Ni, Sn and Pb at beam momenta of 0.71, 0.84, 1.00, 1.36, 1.58 and 2.00 GeV/c. Additionally measurements have been made for Al, ^{120}Sn, Ho and ^{208}Pb at momenta of 0.84, 1.00, 1.36 and 1.58 GeV/c. The ratio of π^- to π^+ reaction cross sections has been analysed in terms of neutron density distributions using the Watson multiple-scattering theory. The effects of second-order contributions and of the various choices of wave equation have been considered. It is found that the distributions of neutrons and protons in heavy nuclei must have very similar radial parameters. Good agreement is obtained between the measured and calculated values for the reaction cross sections, without any adjustment of parameters.

E | NUCLEAR REACTIONS C, Al, Ca, Ni, Sn, ^{120}Sn, Ho, Pb, ^{208}Pb(π^-), (π^+), E = 584, 713, 870, 1228, 1447, 1856 MeV; measured σ_A; deduced neutron density. Enriched and natural targets.

1. Introduction

The distribution of nucleons in the nucleus has been a topic of considerable interest for many years. The proton distribution has been studied for a wide range of nuclei from measurements of elastic electron scattering and X-ray emission from muonic atoms. Because these data are now obtained with relatively high accuracy and the electromagnetic interaction is well understood, it is generally thought that the proton distribution is quite precisely known. In fact, particularly for measurements at moderate momentum transfers, reliable information has been obtained for a certain middle region of the nucleus (which is usually taken to be the transition region in which the density falls from 90 % to 10 % of some average central value), while the extreme inner and outer regions are practically undetermined [44]).

† On leave from The Hebrew University, Jerusalem, Israel.
†† On leave from NPRL, Pretoria, South Africa.
‡ Now at University of Minnesota, USA.
‡‡ Now at University of Sheffield, UK.

Comparable measurements for neutron distributions must be carried out with strongly interacting probes but these interact with both the protons and the neutrons in the nucleus. Recent studies of neutron distributions have been based on methods such as the investigation of the optical potential for scattering of medium-energy protons [1]) or alpha particles [2]) by nuclei, analyses of cross sections for very-high-energy pions [3]) on nuclei, studies of Coulomb displacement energies [4]) or the analysis of neutron transfer reactions [5]). The first two of these methods determine the whole of the nuclear matter distribution and whilst the results depend critically on the treatment of the effective interaction they suggest that for heavy nuclei the distribution of neutrons extends slightly beyond that of the protons. The same conclusion is obtained from the analyses of high-energy cross sections, where again the results actually determine the whole of the nuclear matter distribution but the particle-nucleus interaction is better known than at the lower energies. The last two methods give information which relates only to certain specific neutron orbitals in the nucleus and further assumptions are necessary before parameters describing the full neutron distribution can be derived.

Interest in the neutron distribution is enhanced by the fact that for medium-weight and heavy nuclei the number of neutrons N is larger than the number of protons Z. Simple single-particle model calculations [6]) suggest that for a heavy nucleus such as lead the neutrons could extend beyond the protons by 0.3 to 0.4 fm, thus forming a "neutron halo". More sophisticated shell-model calculations using Hartree-Fock techniques [7]), however, reduce this difference to 0.1–0.2 fm. Alternatively it can be argued that because the neutrons are required to counterbalance the long-range Coulomb repulsion and because the interaction between unlike particles is greater than that between like particles the neutrons and protons will tend to have similar spatial distributions. It is therefore of great interest to determine as accurately as possible the parameters of the neutron density distribution.

The method used in the present experiment is based on a suggestion by Piccioni and the experiment of Abashian *et al.* [8]). It uses the fact that at certain momenta around 1 GeV/c π^- mesons interact more strongly with protons than with neutrons whilst π^+ mesons interact more strongly with neutrons than with protons. As a result the ratio of reaction cross sections for π^- and π^+ mesons incident on a nucleus will depend on the relative distribution of neutrons and protons. Since the proton distribution is considered to be known, a measurement of the ratio of the reaction cross sections for incident π^- and π^+ mesons yields information on the neutron distribution.

There are many differences between the present work and the previous experiment [ref. [8])]. Two of the more important are that the experimental uncertainties have been reduced by a factor of two and the experiment has been performed at several beam momenta and for a wide range of target nuclei. The theoretical analysis of the present experiment is also an improvement on the previous work [9]) as it uses more recent developments in scattering theory. It is interesting, however, to note that more recent

analyses of the old experimental results made by Elton [10]) and by Auerbach *et al.* [11]) have confirmed the conclusions of the original investigators that the neutron and proton distributions in heavy nuclei must be very similar.

Sect. 2 explains in more detail the ideas that form the basis of this experiment and sect. 3 gives a detailed description of the apparatus and experimental technique. The results are presented in sect. 4. Sect. 5 deals with the theoretical aspects of the pion-nucleus interaction and with the calculation of the reaction cross sections. The interpretation of the measured cross sections and ratios in terms of nuclear density distributions is discussed in sect. 6 and the conclusions are presented in sect. 7.

2. Method

One of the characteristics of the pion-nucleon interaction in the momentum region around 1 GeV/c is that the π^--p total cross section is different from the π^+-p total cross section and at certain momenta they differ by more than a factor of two. By charge independence the π^--p and π^+-n total cross sections are equal and similarly the π^+-p and π^--n cross sections are equal. The magnitude of these elementary pion-nucleon cross sections is such that the mean free path of pions in nuclear matter is of the order of 2 fm.

In discussing the method used in this experiment it is convenient to describe pion-nucleus interactions using an impact approach which has considerable validity at the energies used in this work. The description of the method in this section will be purely qualitative; a quantitative description of some features in terms of impact parameters is given in subsect. 6.1.

For small impact parameters the pions will almost always interact and the corresponding region of the nucleus can therefore be considered to be "black". However as the impact parameter increases and becomes comparable to the nuclear radius both the local nuclear density and the effective "thickness" of the nucleus decrease. The probability of an interaction at large impact parameters then becomes a function of the local neutron and proton densities and the pion-nucleon cross sections. These large impact parameters can give significant contributions to the reaction cross section. As a result the difference between the π^- and π^+ nuclear reaction cross sections will depend on the different pion-nucleon total cross sections and on the densities of neutrons and protons in the region of large impact parameters, i.e. in the surface of the nucleus. In fact, as is shown in subsect. 6.1, the difference between the π^- and π^+ reaction cross sections is almost entirely due to the differing contributions from the region of impact parameters corresponding to the nuclear (50 % density) radius. The difference between the cross sections is therefore a sensitive probe of the relative densities of neutrons and protons in the surface region and hence can be used to measure the parameters of the neutron distribution.

The absolute magnitude of the difference between the π^- and π^+ reaction cross sections depends not only on the difference between the neutron and proton density

distributions but also on the size of the nucleus and on the elementary pion-nucleon cross sections. Much of this dependence can be removed by considering instead the ratio of π^- to π^+ reaction cross sections and it is then the difference between this ratio and unity which is a measure of the relative neutron and proton distributions.

We have so far only discussed pion-nucleus reaction cross sections. In principle measurements of total cross sections could give similar information. However, in sect. 3 we show that for experimental reasons total cross sections cannot be measured over the momentum region covered by this experiment. In any case from the point of view of analysing the results measurements of the reaction cross section are to be preferred. If the cross section is calculated using a pion-nucleus optical model, then it is found that the reaction cross section depends almost entirely on the imaginary part of the potential.

This potential is given in its simplest form (see sect. 5) by

$$V^{\pm}(r) = -\frac{2\pi\hbar^2c^2}{E_L}[f^{\pm}(0)Z\rho_p(r)+f^{\mp}(0)N\rho_n(r)], \tag{2.1}$$

where E_L is the total energy of the pion in the laboratory system and $f^{\pm}(0)$ is the forward $\pi^{\pm}$ proton scattering amplitude in the laboratory. The imaginary part is obtained using the optical theorem which gives

$$\text{Im } V^{\pm}(r) = -\frac{\hbar^2c^2k_L}{2E_L}[\sigma_T^{\pm}Z\rho_p(r)+\sigma_T^{\mp}N\rho_n(r)], \tag{2.2}$$

where k_L is the wave number of the pion in the laboratory system, $\rho_p(r)$ and $\rho_n(r)$ are the nuclear density distributions for protons and neutrons respectively, normalized to unity and $\sigma_T^{\pm}$ is the $\pi^{\pm}$ proton total cross section. As these pion-nucleon total cross sections are well known, the imaginary potential (2.2) depends on $\rho_p(r)$ and $\rho_n(r)$ which we wish to compare. Therefore the pion-nucleus reaction cross section σ_R is the most suitable quantity to analyse.

A full account of the calculations is given in sect. 5. Before an expression such as (2.2) can be used for the calculation of pion-nucleus reaction cross sections, the Fermi motion of the nucleons inside the nucleus must be taken into account. This is described in subsect. 5.5. The results of this averaging are shown in fig. 1 together with the free pion-nucleon total cross sections. It is seen that although the Fermi averaged cross sections have a much smoother behaviour than that of the free cross sections, there are still sufficiently big differences between the π^- and π^+ cross sections to make the present method a promising one. Before starting the present experiment an extensive series of calculations was performed which supported the above expectations. The results of some similar calculations have been published by Sternheim and Auerbach [ref. [12])] after the completion of the present experiment.

The program of the present experiment can be understood from an inspection of fig. 1. Three momenta 0.71, 0.84 and 1.00 GeV/c were chosen where the Fermi averaged π^- and π^+ proton cross sections are very different, resulting in a strong depen-

dence of the ratio $\sigma_R(\pi^-A)/\sigma_R(\pi^+A)$ on the difference between the proton and neutron density distributions. Two additional momenta, 1.36 and 1.58 GeV/c were chosen because here the Fermi averaged pion-nucleon total cross sections are equal and therefore the ratio is independent of the difference between the proton and neutron distributions over a wide range. These points serve, therefore, as check points on the comparison between experiment and theory. The momentum of 2.00 GeV/c has been included because of the interest in the results at higher energies.

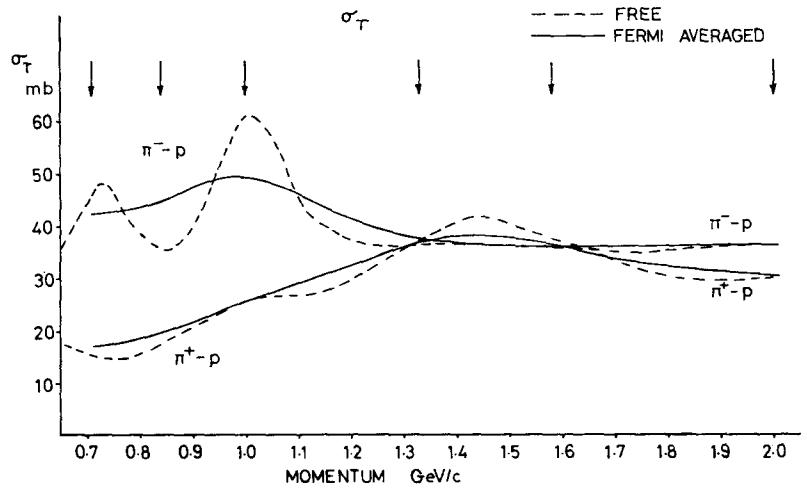

Fig. 1. The pion-nucleon total cross sections as a function of incident momentum. The Fermi-averaged values were obtained using the procedure outlined in sect. 5.

The nuclei chosen were C, Al, Ca, Ni, Sn, Ho and Pb. The nuclei Sn and Pb were studied also for the separated isotopes ^{120}Sn and ^{208}Pb. The light nuclei C and Ca in particular (with 98.9 % of ^{12}C and 97.0 % of ^{40}Ca, respectively) served as additional check points because it seems safe to assume that in these nuclei the protons and neutrons must have almost identical distributions. An agreement between experiment and theory for these nuclei considerably increases the reliability of any conclusions regarding the heavy nuclei which were the prime aim of this experiment.

The present method offers considerable advantages over previous methods of determining neutron distributions [1-5]). Firstly the existence of two different projectiles which at certain momenta interact preferentially with neutrons or protons respectively; secondly the elimination of several theoretical and experimental uncertainties by comparing ratios; and finally the high incident energy enabling the pion-nucleus interaction to be determined reliably from the pion-nucleon interaction.

3. Experimental

3.1. PRINCIPLES

The experiment consisted of a measurement of the reaction cross section for pions on a particular target nucleus. The nuclear reaction cross section is the cross section

for any interaction of a particle with a nucleus other than elastic Coulomb or nuclear scattering. All other processes, which generally involve either the excitation or breakup of the interacting nucleus, are included in the reaction cross section. The total cross section is similarly defined as the cross section for the occurrence of any interaction (including nuclear elastic scattering) other than elastic Coulomb scattering.

Reaction cross sections are usually measured using the conventional transmission technique, which will first be described for the ideal case. A narrow parallel beam of pions incident on a target is detected by a counter placed after the target. The counter is of such a size that any pion involved in a reaction is absorbed or scattered out of the beam and is thus not detected, whereas any pion which undergoes either Coulomb or elastic nuclear scattering is deflected through only a small angle and is detected. If N_2 pions are detected in the transmission counter for a beam of N_1 particles incident on the target then

$$N_2 = N_1 \mathrm{e}^{-n\sigma_R t}, \tag{3.1}$$

where t is the thickness of the target and n the number of scattering nuclei per unit volume. The reaction cross section is then given by

$$\sigma_R = -\frac{1}{nt} \log \frac{N_2}{N_1}. \tag{3.2}$$

The description as presented above is simplified and in practice there are two important effects which need to be included. Firstly some of the reaction products due to inelastic interactions will be detected in the counter, and secondly some of the incident particles will be elastically scattered outside the transmission counter. The cross section for scattering outside a counter subtending a solid angle Ω at the target is then related to the reaction cross section σ_R by

$$\sigma(\Omega) = \sigma_R - \int_0^{\Omega} \frac{\mathrm{d}\sigma}{\mathrm{d}\Omega_{\mathrm{inel}}} \mathrm{d}\Omega + \int_{\Omega}^{4\pi} \frac{\mathrm{d}\sigma}{\mathrm{d}\Omega_{\mathrm{el}}} \mathrm{d}\Omega, \tag{3.3}$$

where the differential elastic scattering cross section $\mathrm{d}\sigma/\mathrm{d}\Omega_{\mathrm{el}}$ includes both nuclear and Coulomb scattering.

The normal technique used to obtain the reaction cross section is to measure $\sigma(\Omega)$ over a range of solid angles in the region where the elastic scattering contribution is small and after correcting for this to extrapolate the measurements to zero solid angle. In order to keep the elastic scattering corrections small, measurements should be made at large solid angles, since elastic scattering is generally strongly peaked in the forward direction. However, it is then necessary to extrapolate the measurements over a large solid angle range so implying some assumptions about the form of $\mathrm{d}\sigma/\mathrm{d}\Omega_{\mathrm{inel}}$ at small solid angles. In practice it is usually possible to choose the range of solid angles so that neither of these restrictions is too severe.

To enable measurements to be made at several solid angles simultaneously, an array of transmission counters is used, each counter having a different diameter and

hence subtending a different solid angle at the target. It is also necessary to correct for attenuation in the air and other materials surrounding the target and transmission counter. This is most easily achieved by making measurements of the transmission when the target is removed. If primes are used to denote "target-out" quantities and if

$$N_2' = N_1' \mathrm{e}^{-s},$$

then

$$N_2 = N_1 \mathrm{e}^{-n\sigma(\Omega)t}\mathrm{e}^{-s},$$

$$\sigma(\Omega) = -\frac{1}{nt} \log \frac{N_2}{N_1} \frac{N_1'}{N_2'}. \tag{3.4}$$

Since the sizes of the transmission counters are generally chosen to be sufficiently large so as to include the major fraction of the particles undergoing elastic scattering, such a measurement is generally known as a bad geometry transmission experiment. For a measurement of the total cross section a good geometry experiment would be required where the solid angles subtended by the transmission counters are chosen so as to include the major part of the Coulomb scattering but to exclude particles which have undergone nuclear scattering. At high energies and for heavy (large) nuclei, the nuclear scattering becomes sharply forward peaked and it is extremely difficult to separate the nuclear from the Coulomb scattering. It is for this reason that total cross sections cannot be measured for medium weight and heavy nuclei over the incident pion momentum region covered in the present experiment.

3.2. BEAM LINE AND MOMENTUM DETERMINATION

The experiment was carried out using a pion beam from the 7 GeV proton synchrotron NIMROD. An overall layout of the equipment and associated beam line is shown in fig. 2. Pions and other charged particles produced by a 1 cm × 1 cm × 5 cm long tungsten target positioned inside the Nimrod vacuum vessel were collected by the quadrupole doublet Q1, Q2 and steered using the magnet M1 onto a scintillation counter hodoscope H. A further magnet M2 selected the momentum of the beam and the two quadrupole doublets Q3, Q4 and Q5, Q6 were then used to focus the beam at the target position.

The beam spot was approximately 4 cm diameter at the final target position with a divergence of ± 20 mrad. Typical intensities for π^- beams with 3×10^{11} protons/burst incident on the production target were between 2×10^3 and 2×10^4 pions/burst over an area of 3.1 cm^2 (the size of the final beam defining counter at the experimental target position), depending on the beam momentum. For the π^+ beams the intensities were rather lower, by about a factor of 5; however, the positive pion beams were accompanied by a relatively large flux of protons so that the total charged particle rates for the two polarities were rather similar. For both beam polarities, muons and electrons were also present as a contamination with an intensity of about 20 % of the pion rate.

The setting up of the various beams was straightforward. Two sets of Charpak

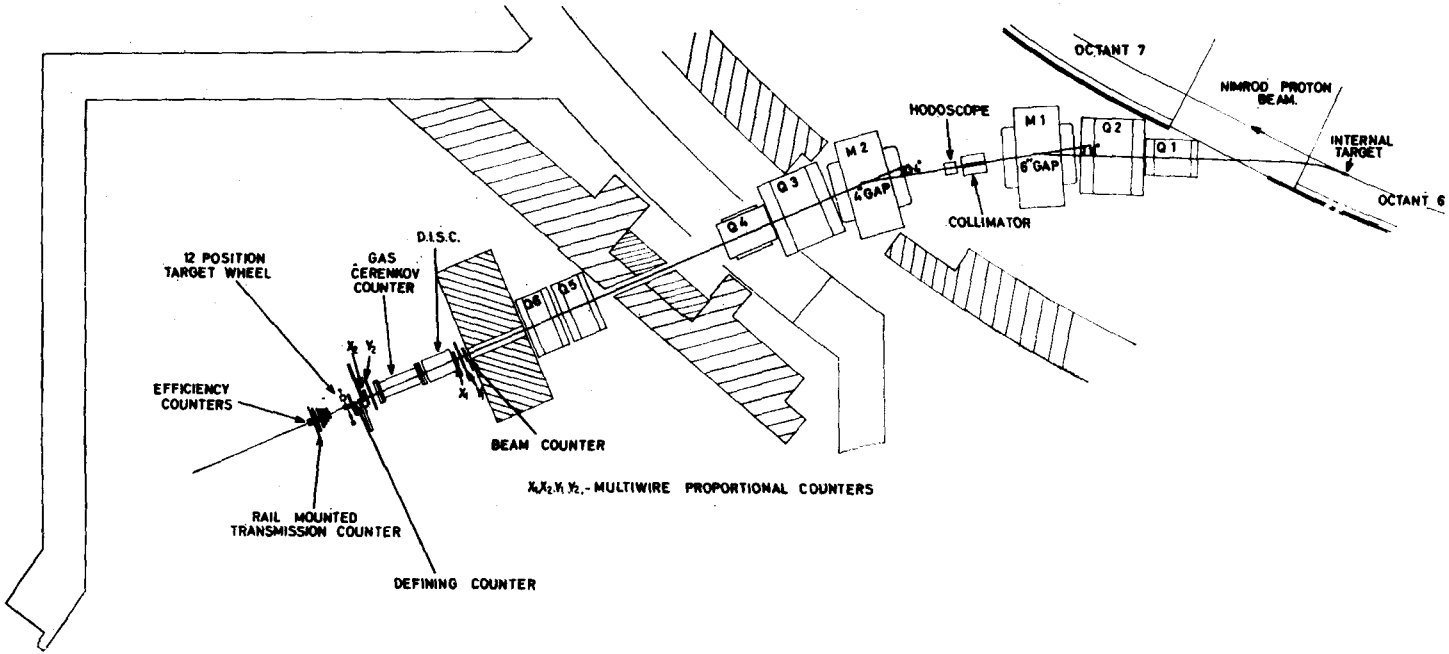

Fig. 2. Overall layout of beam-line and equipment.

counters [13]) were used to measure the beam profile after Q6 and at the final target position. Generally the final quadrupole and magnet currents used were very close to the predicted values obtained in the beam line design which used the computer program TRANSPORT [14]).

Measurements were made using beams over the momentum region from 0.7 to 2.0 GeV/c. The beam momentum was defined by the positions of the hodoscope counter H, the position of the experimental target and the integrated magnetic field $\int B\mathrm{d}l$ along the beam trajectory. Hall-effect field probes were used to monitor the magnetic fields in both the M1 and M2 magnets. A calibration of the beam momentum to better than 1 % in terms of the magnetic field at a standard position in the M2 magnet had previously been made by another experimental team using the floating wire technique, and this was used in the early stages of the present experiment. This calibration was checked and confirmed, however, by making measurements with the present apparatus of the total cross section for π^--p scattering using the CH_2-C difference technique. At momenta of 720 MeV/c and 1002 MeV/c there are resonances in the π^--p total cross section. Careful measurements of the π^--p cross section were taken over the resonances and using their positions as obtained from an analysis of published measurements, the beam momenta could be determined to an accuracy of ± 0.3 %. These momenta agreed with those obtained from the previous calibration to within the error. Allowing for the uncertainty in the positions of the resonances the beam momenta as quoted for the present experiment therefore have an overall accuracy of ± 0.4 %. The spread in momentum of particles incident on the target for a given momentum setting was ± 2 %.

3.3. BEAM DEFINITION AND PARTICLE IDENTIFICATION

A schematic layout of the counters and associated equipment is given in fig. 3. The final beam-defining counters B_3 and B_4 positioned just before the experimental target had diameters of 4.0 cm and 2.0 cm respectively. The incident beam was defined by the coincidence $B_1 H B_2 B_3 B_4$. Two adjacent elements of the counter hodoscope H were used for π^+ beams and three adjacent elements for π^- beams. This difference was due to the different acceptances of the beam line for π^+ and π^-.

For particle identification a differential Čerenkov counter (D) of the DISC type [15]) and a gas threshold Čerenkov counter were used. The DISC consisted of a 5 cm long radiator of tetrafluoropropanol viewed by nine selected RCA 8575 photomultipliers. At momenta of 1.58 and 2.00 GeV/c the photomultiplier signals were used in nine-fold coincidence to give the DISC signal D. At the lower momenta, where the discrimination against protons was easier due to the differences in times of flight, the signals from sets of three adjacent photomultipliers were combined and the three resulting outputs used to form a three-fold coincidence. The function of the DISC counter was principally to select pions and to reject protons and K-mesons. To reject muons and electrons a 67 cm long gas threshold Čerenkov counter was used. The Čerenkov radiator was ethylene gas at a pressure that was varied with the beam momentum,

such that both muons and electrons were detected. The Čerenkov light was viewed through a thin 45° mirror by an RCA developmental photomultiplier type C70133B. The output signal G was placed in anticoincidence with the output of the DISC counter. The signal for a beam pion was therefore defined by the coincidence $B_1 H B_2 B_3 B_4 D\bar{G}$. Whilst the DISC counter gave very adequate rejection of protons in the beam, some additional discrimination was provided at the lowest momenta by their increased time of flight (45.7 nsec for protons compared with 33.7 nsec for pions at 1.00 GeV/c) over the 10 m flight path between $B_1 H$ and B_2. For momenta below 1.36 GeV/c it was possible to reject almost all the proton events using this method alone. With the whole system as described above the contamination of beam signals by particles which were not pions was estimated to be certainly less than 10^{-4}.

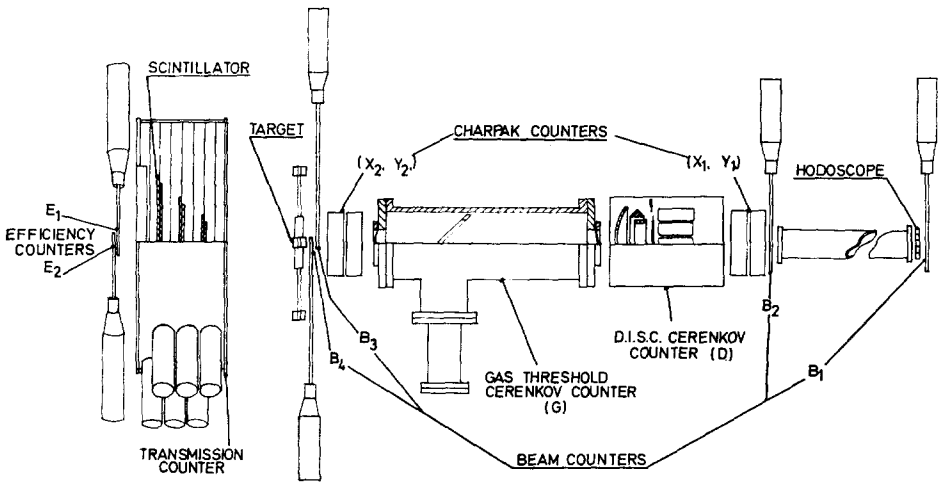

Fig. 3. Counter and detection system.

3.4. TRANSMISSION COUNTERS

The transmission counters consisted of six circular disks of NE102A scintillator with diameters of 18, 24, 33, 40, 51 and 59 cm respectively. The first five counters were 0.95 cm thick and the final one 1.25 cm thick. The distance between the centre of the front counter and the centre of the back counter was 21.44 cm. The usual light-guide system was not used. Instead the counter disks were mounted in a cylindrical vessel 105 cm dia × 40 cm long which was divided into six light-tight cells by layers of aluminized 0.13 mm thick melinex sheet. The disks were bonded one to each side of alternate cell walls and were viewed from the edge by RCA 8575 photomultipliers mounted on the circular face of the enclosing vessel. To improve the light collection a strip of aluminized melinex with a width equal to that of the cell was wrapped around the edge of the scintillator disk and tapered to match the photomultiplier aperture. A schematic diagram of the counter is given in fig. 3.

The advantage of this design of transmission counter is that there is very little extraneous material in the path of the beam and as light-guides are not used, there is no problem with Čerenkov radiation. Despite the lack of light-guides the efficiencies of the counters were found to be remarkably good. In tests two small counters, E and F, consisting of cubes of scintillator of side 0.4 cm were placed either side of the transmission counter T. By forming the double and triple coincidences EF and EFT the efficiency of the transmission counter is then given by η = EFT/EF. By scanning the E and F counters over the surface of the transmission counter, the efficiency (typically 99.95 %) was found to be extremely uniform and only dropped to 99.90 % at a distance of 0.2 cm from the edge of the counter. It was also found that the effective sizes of the various counters agreed to within ± 0.2 mm with their physical dimensions.

Signals from the six transmission counters were used with the beam pulse B to form the five sets of three-fold coincidences BT_iT_{i+1} (i = 1, 5). Using coincidences between adjacent pairs of transmission counters considerably reduced the contribution from noise pulses in the transmission counter to the random coincidence rate. With the transmission counter operated in this way it was possible to make measurements simultaneously at five different solid angles.

The transmission counter was mounted on a trolley which could be moved backwards and forwards relative to the target position. The counter assembly could be positioned to an accuracy of 0.1 mm. At a distance of 40 cm from the target the transmission counters covered solid angles in the range from 153.5 msr to 499.3 msr. Measurements were made with the counter at four different distances, between 40.0 cm and 46.7 cm from the target. In this way, it was possible to cover 20 solid angles in the region from 113 msr to 500 msr with considerable overlap between the range of solid angles covered at each position.

Two counters E_1 and E_2 were used to monitor continuously the efficiencies of the transmission counters by forming the coincidences BE_1E_2 and $BT_iT_{i+1}E_1E_2$. The efficiency of the T_iT_{i+1} pair is then given by $\eta_{i,i+1} = BT_iT_{i+1}E_1E_2/BE_1E_2$. A small dependence of this measured efficiency on the beam rate was found but at no time its value drop below 99.8 %.

3.5. ELECTRONICS AND DATA ACQUISITION SYSTEM

The electronics system was conventional and will not be described in detail. Typical discriminator dead-times were 20 to 25 nsec and resolving times were 5 nsec for the coincidence B and 20 nsec for the coincidence BT_iT_{i+1}. The maximum counting rate which the scalers would handle was 50 MHz.

The principal correction for random events has to be made for those cases where a correctly identified beam pion is scattered by the target outside the acceptance of the transmission counters whilst the corresponding signal B is in random coincidence with a stray particle passing through some or all of the transmission counters. This contribution was measured by delaying a $B\overline{T_iT_{i+1}}$ signal and forming a coincidence

between it and the T_iT_{i+1} signal to give $\theta_i = (\overline{BT_iT_{i+1}})_\Delta T_iT_{i+1}$ where the subscript Δ indicates a signal delayed by one r.f. period of the accelerator. Since the major contribution to the random events was from two particles traversing the beam line within the resolving time of the BT_iT_{i+1} coincidences a significant reduction in this quantity was obtained by vetoing all events where two particles pass through the B_3 counter within 50 nsec of each other. A signal V indicating that an event of this type had occurred was produced by essentially measuring the pulse length from an updating discriminator and this was included in anticoincidence in the main beam signal.

The principal quantities which were scaled (denoted by Greek symbols) and the corresponding coincidences required were

Beam signal

$$\begin{aligned}
&\beta = B = B_1 HB_2 B_3 B_4 D\overline{GV},\\
&\beta\tau_i = BT_iT_{i+1} \text{ for } i = 1, 5,\\
&\beta\tau_i\varepsilon = BT_iT_{i+1}E_1E_2 \text{ for } i = 1, 5,\\
&\beta\varepsilon = BE_1E_2,\\
&\theta_i = (\overline{BT_iT_{i+1}})_\Delta T_iT_{i+1}.
\end{aligned} \tag{3.5}$$

The instantaneous beam rate was measured by the signal $B_\Delta T_5 T_6$ and the quantity $B_\Delta T_5 T_6/B$ formed a convenient measure of the average beam rate during an experimental measurement. A number of other auxiliary quantities were also scaled and used to monitor the operation of the DISC and gas threshold counters.

The scalers were interfaced using the CAMAC system to a PDP-8 computer. In this way the scaled quantities were read directly by the computer and stored on 7-track magnetic tape. The computer also calculated and printed the measured cross-section values and a variety of monitoring quantities such as the transmission counter efficiencies. Using the notation given above for the scaled quantities, the measured transmission ratio, corrected for random events is

$$\alpha_i = (\beta\tau_i - \theta_i)/\beta \tag{3.6}$$

and the counter efficiency is

$$\eta_i = \frac{\beta\tau_i\varepsilon}{\beta\varepsilon}. \tag{3.7}$$

The true transmission ratio is obviously α_i/η_i. If primes are again used to denote "target-out" quantities then by analogy with eq. (3.4) the cross section at a solid angle Ω_i is given by

$$\sigma(\Omega_i) = \frac{1}{nt}\log\frac{\eta_i}{\alpha_i}\frac{\alpha_i'}{\eta_i'}. \tag{3.8}$$

The corresponding error is given by

$$\Delta\sigma(\Omega_i) = \frac{1}{nt}\left[\frac{1-(\alpha_i/\eta_i)}{(\alpha_i/\eta_i)\beta} + \frac{1-(\alpha_i'/\eta_i')}{(\alpha_i'/\eta_i')\beta'}\right]^{\frac{1}{2}}, \tag{3.9}$$

It is perhaps worth commenting at this stage that the measured cross sections for different solid angles at a given transmission counter setting are not statistically independent since for example all the $\beta\tau_i$ counts are contained in $\beta\tau_{i+1}$. This feature has to be kept in mind when simultaneously fitting several sets of data taken at different transmission counter settings.

3.6. TARGETS

The majority of the targets used were of natural isotopic composition and in the form of cylinders of diameter 4 cm with their length along the beam direction chosen so as to give a transmission of the order of 90 %. The Ca target was 2.5 cm in diameter. Separated isotope targets of ^{120}Sn and ^{208}Pb were also used. For these targets, in order to make the best use of the limited quantity of material available, the diameter was chosen to be 2.5 cm and the transmission was approximately 96 %. A list of the target materials and their properties is given in table 1.

TABLE 1
Target materials

Element	A	Surface density (g/cm^2)
C	12.01	6.21
Al	26.98	8.10
Ca	40.08	8.07
Ni	58.71	17.69
Sn	118.69	14.57
^{120}Sn	119.90	7.86
Ho	164.93	13.09
Pb	207.19	22.69
^{208}Pb	207.98	5.44

3.7. MEASUREMENTS

Two sets of Charpak counters [13]) were used to check that the beam was on-axis and focussed at the target position when setting up the beam line. The DISC counter and gas threshold counter were then set up using standard procedures. With a given beam momentum, polarity and transmission counter setting, a series of runs were made for the different targets and the "target-out" data. About one "target-out" run was made for every four "target-in" runs. A typical run was for between 10^7 and 10^8 β-counts, giving statistical errors of approximately 0.1 % and took between 40 and 100 min. When data for a particular beam polarity and counter position had been taken, the beam polarity was changed and the procedure repeated. When this data was complete the counter position was changed and the above procedure again repeated. This scheme which involved changing either the counter position or beam polarity (but not both) at the end of a series of runs was devised in an attempt to reduce possible systematic errors.

Since the cross sections as a function of solid angle (corrected for counter efficiencies and random rates) were available at the end of each experimental run from the on-line computer, they could be compared immediately with the values obtained for the same target and beam polarity but at other counter positions. In this way the quality of the data was continuously monitored and any possible malfunction of the apparatus could be detected immediately.

At each momentum, measurements were also made of the π^+-p and π^--p total cross sections using the CH_2-C difference method. In all cases the results were in satisfactory agreement with published data giving confidence in the results obtained for other targets.

3.8. DATA ANALYSIS

The procedure used in analysing the raw experimental data will be briefly described and then discussed in detail. It was first necessary to correct the raw measurements for rate dependent effects in the electronics system and for the elastic scattering contribution. The corrected measurements were then extrapolated to zero solid angle and corrections applied to the extrapolated value for a dependence on the size of the target and for the decay of pions between the gas threshold counter and the target position. The extrapolation procedure is described in the next section and a detailed discussion of the various corrections then follows.

3.8.1. Extrapolation procedure. The cross-section values as a function of solid angle were fitted by a simple polynomial using the least-squares method and extrapolated to zero solid angle. In the majority of cases it was found that a second-order polynomial was sufficient but in some cases third order was required. In those cases where a second-order polynomial clearly gave a good fit to the data the results from the third-order polynomial were almost identical. To avoid uncertainties due to the choice of the order of the polynomial the final extrapolated values were obtained in all cases from third-order fits to the data.

Using this procedure the reaction cross sections for π^- and π^+ mesons were obtained and their ratio was calculated by a simple division. However it was also possible to obtain the value of this ratio in a more direct way. In this method the cross sections as a function of solid angle were obtained as described above. The ratio of the individual π^- to π^+ cross sections was then extrapolated to zero solid angle using the polynomial fitting technique. In this way the value of the ratio was obtained directly. This method had two significant advantages; it involved only one extrapolation to zero solid angle and it was found that a lower order of polynomial could be used. In this way the uncertainties due to the extrapolation procedure were reduced and the ratios obtained in this way have significantly smaller errors than those obtained from individual reaction cross-section values. The values of the ratio obtained from the two methods are in good agreement.

Using this method a first-order polynomial fit to the data was satisfactory for almost all cases. However when considering all the data together a small systematic

difference was found between the extrapolated values from second-order and first-order fits to the data. Consequently it was felt that the results obtained using second-order polynomials would be more reliable and these were used for all values of the ratio presented in subsect. 4.2.

3.8.2. Corrections to the data. The various corrections which had to be applied to the data will now be discussed separately and in detail.

(i) *Rate effect.* Extensive tests of the experimental equipment showed a small dependence of the measured cross sections on the beam rate. The beam rate was measured as described in subsect. 3.5. A correction for this effect was applied to the experimental data in the following way.

Measurements were made of the observed cross section as a function of beam rate for one or more targets and for one transmission counter position. These measurements were made at each momentum and for both beam polarities. This latter point is important since the ratio of identified pions to the total number of incident particles changes markedly between π^- and π^+ beams due to the large number of protons present in the latter case.

The measured cross sections as a function of beam rate were then fitted by a straight line using the least-squares method. From the slope of this line and its intercept at zero rate the relative correction to the cross sections for a unit change of rate was determined. Using this factor and the beam rate measured during each experimental run it was then possible to correct each individual cross-section point for rate effects. The uncertainty in the rate correction was also included in the errors on the final cross-section values. A typical correction for rate effects was 0.5 % of the cross-section value and the additional error due to the correction was ± 0.2 % of the value.

(ii) *Elastic scattering.* After correcting the individual cross-section points for rate effects it was then necessary to apply a correction for those elastically scattered pions which missed the transmission counter. This correction which includes both Coulomb and nuclear elastic scattering is clearly largest at the smallest solid angles. As the differential elastic scattering of pions by nuclei has not been measured for the momentum region covered by this experiment, it was necessary to use theoretically predicted values. This was done using the computer programs and formalisms discussed in detail in sect. 5. Using values for the Fermi-averaged pion-nucleon total cross sections discussed in subsect. 5.5 and assuming that the neutron distribution has the same radial parameters as the proton distribution, the differential scattering cross sections were calculated using the computer program ABACUS-M. Using these differential scattering cross sections the correction for elastic scattering was calculated as in eq. (3.3) and then applied to the individual measured values.

This correction is largest at the lowest momenta and for the heaviest nuclei. For Pb at 0.71 GeV/c the correction was typically 4 % at the smallest solid angle point. For momenta above 1 GeV/c, the elastic scattering correction was very small being typically much less than 1 %.

At this stage the results were extrapolated to zero solid angle.

(iii) *Target size.* A correction to the extrapolated cross sections and ratios had to be made for a dependence of these results on the diameter of the target. As the separated isotope targets (^{120}Sn and ^{208}Pb) had a smaller diameter than the others used in this work, the size of the B_4 counter was chosen to be just smaller than the size of these smallest targets. However, when the larger targets were in use it was possible for events to occur where a pion passed through the B_3 counter but not the B_4 counter. If the pion then interacted in the target and produced a backward going charged particle this could pass through the B_4 counter so simulating a true event. Measurements of the dependence of the cross section on the target diameter were made for a few representative nuclei at each momentum and the extrapolated results corrected accordingly. The size of this correction for the reaction cross sections was typically 1 % and the uncertainty in the correction ± 0.3 % in absolute value. For values of the ratio the correction was typically 0.1 % and the uncertainty 0.1 %.

(iv) *Pion decay.* Finally a correction had to be made to the absolute cross sections to allow for the decay of pions into muons (which do not interact in the target) between the gas threshold counter and the target position. This correction was small, being largest at a momentum of 0.71 GeV/c where it was 1.3 %, and smallest at 2 GeV/c where it was 0.6 %. This correction has no effect on the values of the ratio of cross sections since it is the same for both π^+ and π^- mesons.

3.8.3. Errors. The errors on the individual cross sections were calculated using eq. (3.9). The error on the extrapolated value was obtained from the error on the first coefficient of the polynomial given by the least-squares fitting procedure. This error was typically between 0.1 and 0.2 % of the cross-section value.

The additional uncertainty due to the correction for rate dependent effects was obtained from the fitting procedure used to obtain this correction. A typical correction for rate effects was 0.5 % of the cross-section value with an error of ± 0.2 %.

The uncertainty due to the correction for nuclear elastic scattering is difficult to evaluate since it depends on the various parameters used in the theoretical calculation of the differential scattering cross section. For momenta of 0.71 GeV/c and 0.84 GeV/c where the correction is largest, the additional uncertainty due to this cause was estimated to be ± 0.6 % in the individual reaction cross-section values. However, there is a partial cancellation of these uncertainties in the ratio value and here an uncertainty of ± 0.3 % was estimated. As some of the parameters in these calculations are common to all nuclei at a given momentum an additional systematic error of ± 1 % should be applied to the reaction cross-section values for each momentum at 0.71, 0.84 and 1.00 GeV/c and a systematic error of ± 0.2 % in the ratio values at the same momenta. For the higher momenta the elastic scattering correction was very small and any additional uncertainty, either random or systematic was neglected.

The uncertainty in the correction for the size of the target was evaluated directly from the measurements and was typically ± 0.3 % of the measured reaction cross section. It was felt that the correction for pion decay could be reliably calculated and no additional uncertainty for this effect was included except at a momentum of 0.71

GeV/c where an additional ± 0.1 % was included in the errors for the reaction cross-section values.

The uncertainties due to the various corrections (with the exception of the systematic uncertainties from the elastic scattering correction) were added in quadrature together with the statistical error on the cross section or ratio values. The final results are presented in the next section.

4. Results

Measurements were made of the reaction cross sections of π^- and π^+ mesons for the nuclei C, Ca, Ni, Sn and Pb at 0.71, 0.84, 1.00, 1.36, 1.58 and 2.00 GeV/c. Additionally measurements were made for the nuclei Al, ^{120}Sn, Ho and ^{208}Pb at momenta of 0.84, 1.00, 1.36 and 1.58 GeV/c. The results of the absolute measurements are presented below and the values of the π^-/π^+ ratio of cross sections then follow.

4.1. REACTION CROSS-SECTION VALUES

Values of the reaction cross sections for π^- and π^+ mesons measured in this experiment are presented in tables 2 and 3. Errors on the cross-section values vary typi-

TABLE 2

π^- reaction cross sections
(values in mb)

Momentum (GeV/c)	C	Al	Ca	Ni	Sn	^{120}Sn	Ho	Pb	^{208}Pb
0.71	243±3		608±5	764±6	1221±11			1806±15	
0.84	250±2	433±6	607±5	764±6	1230± 9	1241±10	1583±14	1814±12	1759±40
1.00	264±1	454±3	624±5	772±3	1249± 6	1260±11	1607±13	1808± 6	1810± 9
1.36	254±2	444±3	611±4	771±5	1249± 7	1258±10	1594±10	1817± 9	1806±16
1.58	246±2	444±4	598±5	758±4	1233± 5			1802± 7	
2.00	224±2		550±3	710±4	1164±11			1703±16	

An additional systematic error of ±1 % should be applied to the values for each momentum at 0.71, 0.84 and 1.00 GeV/c. (See text for a discussion of errors.)

TABLE 3

π^+ reaction cross sections
(values in mb)

Momentum (GeV/c)	C	Al	Ca	Ni	Sn	^{120}Sn	Ho	Pb	^{208}Pb
0.71	263±3		587±7	741±8	1187±17			1754±16	
0.84	246±3	429±11	594±9	742±9	1190±10	1221±14	1543±28	1752±16	1764±21
1.00	257±2	451±3	609±5	749±5	1231± 8	1254±10	1606±15	1772± 9	1762±26
1.36	248±3	437±4	599±4	752±5	1217± 9	1223±14	1544±26	1743±13	1742±24
1.58	243±3	435±3	601±5	750±6	1208±11			1736±16	
2.00	224±2		555±5	707±8	1154±10			1670±13	

An additional systematic error of ±1 % should be applied to the values for each momentum at 0.71, 0.84 and 1.00 GeV/c. (See text for a discussion of errors.)

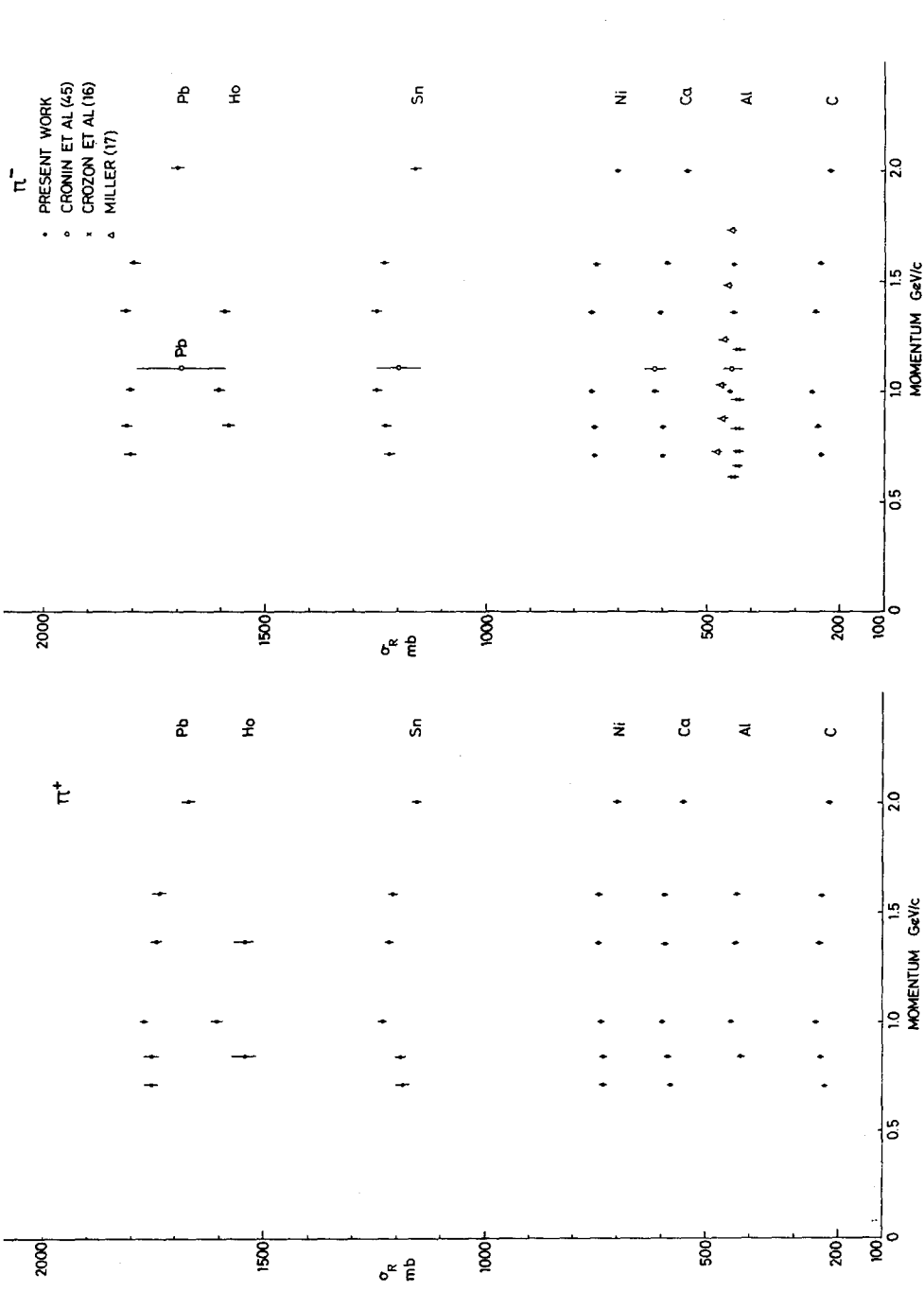

Fig. 4. Reaction cross sections for pions on nuclei from the present work and from previous experiments. For π^- mesons on carbon, see fig. 5.

cally between 0.5 and 1.0 %. The results for the separated isotopes ^{120}Sn and ^{208}Pb have rather larger errors than the values for the natural elements due to the much larger attenuation in the latter case. However, within these errors the values for the corresponding separated and unseparated isotopes show no significant difference.

In figs. 4 and 5 the cross sections are plotted as a function of momentum and compared with other available data. No other measurements appear to have been made in this momentum region for π^+ mesons. For π^- mesons the two other principal experiments are those of Crozon *et al.* [16]) and of Miller [17]). However in these two experiments the pions in the incident beam were not individually identified but rather an overall correction made for muon and electron contamination. This latter correc-

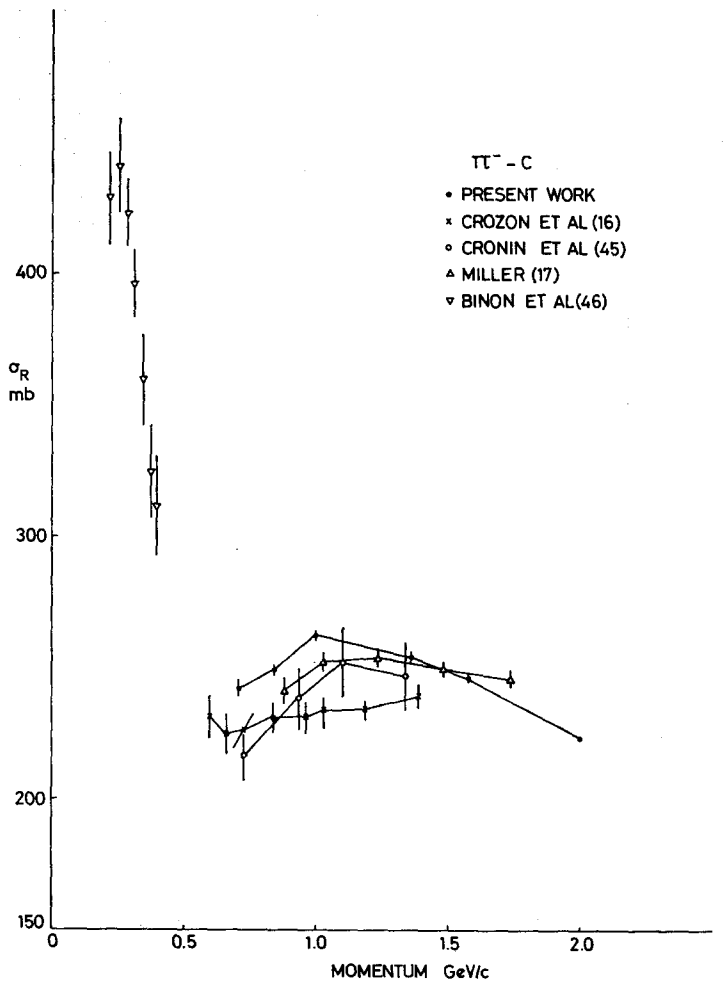

Fig. 5. Reaction cross sections for π^- mesons on carbon from the present work and from previous experiments. The straight lines join values obtained in the same experiment.

tion was measured separately and is dependent on the beam momentum. As a result significant errors can arise using this procedure. The experiment of Crozon *et al.* [16]) also used an annular "halo" counter immediately before the target position to reject

TABLE 4

Coefficients obtained by fitting an equation of the form $\sigma_R = CA^n$ to the experimental data

Momentum (GeV/c)	Polarity	C (mb)	n
0.71	π^-	43.8±2.9	0.699±0.016
0.71	π^+	42.5±2.5	0.699±0.014
0.84	π^-	46.1±2.3	0.688±0.011
0.84	π^+	44.7±1.3	0.689±0.007
1.00	π^-	49.4±1.5	0.677±0.007
1.00	π^+	47.9±1.8	0.679±0.009
1.36	π^-	46.5±1.3	0.689±0.006
1.36	π^+	46.5±1.5	0.683±0.007
1.58	π^-	44.7±1.5	0.696±0.008
1.58	π^+	45.2±2.4	0.688±0.013
2.00	π^-	38.8±1.5	0.712±0.009
2.00	π^+	39.6±2.1	0.704±0.013
Mean value			0.689±0.003

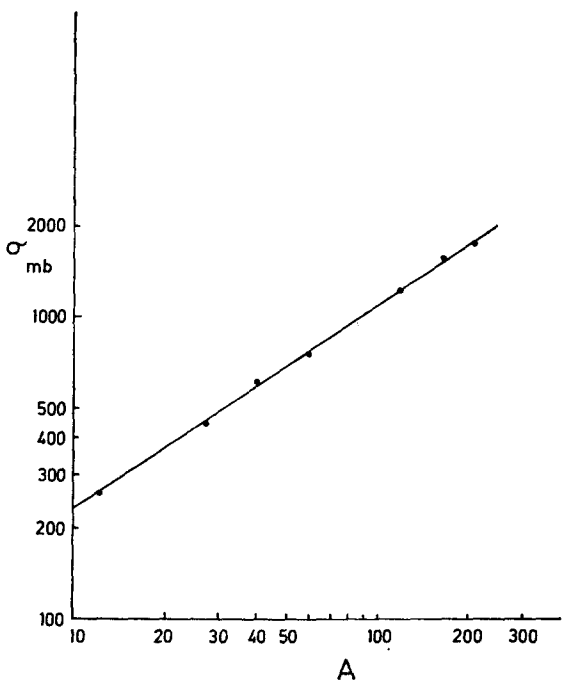

Fig. 6. Logarithmic plot of the measured reaction cross sections for 1.00 GeV/c π^--mesons. The straight line represents the best fit with an expression of the form $\sigma_R = CA^n$ (see table 4).

TABLE 5

Ratio π^-/π^+ calculated from reaction cross sections

Momentum (MeV/c)	C	Al	Ca	Ni	Sn	^{120}Sn	Ho	Pb	^{208}Pb
0.71	1.025±0.015		1.036±0.013	1.031±0.011	1.029±0.015			1.030±0.010	
0.84	1.014±0.012	1.009±0.027	1.023±0.015	1.029±0.013	1.033±0.009	1.017±0.012	1.026±0.020	1.035±0.009	0.997±0.025
1.00	1.027±0.007	1.008±0.009	1.024±0.011	1.031±0.008	1.015±0.008	1.005±0.012	1.000±0.012	1.021±0.006	1.027±0.016
1.36	1.026±0.014	1.016±0.012	1.020±0.010	1.026±0.009	1.026±0.009	1.029±0.014	1.033±0.018	1.043±0.009	1.037±0.017
1.58	1.014±0.013	1.019±0.012	0.995±0.012	1.010±0.010	1.021±0.010			1.038±0.010	
2.00	1.000±0.011		0.991±0.011	1.005±0.013	1.009±0.013			1.020±0.013	

An additional systematic error of ±0.2 % should be applied to the values for each momentum at 0.71, 0.84 and 1.00 GeV/c.
(See text for a discussion of errors.)

TABLE 6

Ratio π^-/π^+ of reaction cross sections obtained by direct extrapolation of measured ratios

Momentum (MeV/c)	C	Al	Ca	Ni	Sn	^{120}Sn	Ho	Pb	^{208}Pb
0.71	1.018±0.007		1.034±0.007	1.039±0.006	1.029±0.007			1.033±0.006	
0.84	1.019±0.006	1.028±0.013	1.045±0.010	1.035±0.007	1.025±0.007	1.025±0.008	1.033±0.009	1.039±0.005	1.042±0.011
1.00	1.026±0.005	1.009±0.004	1.028±0.005	1.033±0.005	1.013±0.003	1.010±0.005	1.014±0.005	1.025±0.003	1.023±0.009
1.36	1.007±0.007	1.014±0.009	1.015±0.007	1.027±0.005	1.030±0.005	1.032±0.009	1.041±0.009	1.043±0.007	1.045±0.010
1.58	1.006±0.009	1.013±0.008	1.015±0.008	1.020±0.006	1.029±0.006			1.039±0.006	
2.00	1.002±0.006		1.000±0.009	1.006±0.009	1.008±0.008			1.015±0.009	

An additional systematic error of ±0.2 % should be applied to the values for each momentum at 0.71, 0.84 and 1.00 GeV/c.
(See text for a discussion of errors.)

particles outside the defined beam area. It has been the experience in the present experiment that such a system can give rise to low cross-section values. Identified pions interacting in the target may give a backwards going charged particle which gives a signal in the anti-coincidence halo counter and so vetos the event. The magnitude of the effect depends on the sizes and relative positions of the counters and target but can be of the order of a few percent. It is perhaps significant that the results of Crozon *et al.* are low when compared with those found in the present work. Within these limitations the agreement between the various experiments is moderately satisfactory.

A full comparison of the present results with theoretical predictions is made in sect. 6. However, the results have also been fitted to the empirical equation $\sigma_R = CA^n$ and the values of C and n for the various beam momenta are given in table 4. Values for n close to $\frac{2}{3}$ are obtained as is to be expected since at these pion energies the nucleus is essentially "black". Little other theoretical significance can be given to the values of the constants but the formulae may be of use in estimating values of reaction cross sections for other nuclei. The deviation of the measured cross sections from the values given by the formula is typically $\pm 2\,\%$. The experimental results for 1.00 GeV/c π^- mesons are compared in fig. 6 with the predictions of this equation.

4.2. π^-/π^+ RATIO VALUES

The values of the ratio of π^-/π^+ reaction cross sections obtained from the absolute values as discussed above are given in table 5. The values of the ratio obtained using the alternative extrapolation procedure described in subsect. 3.8.1 are given in table 6. It will be noticed that in the latter case the errors on the results (typically 0.6 %) are almost a factor of two smaller than those on the ratios obtained from the absolute cross sections. However, the agreement between the two sets of results is extremely satisfactory, the difference between the values being almost always less than the quoted errors. This agreement gives confidence in the extrapolation procedures used in the two methods. A full analysis and interpretation of these results in terms of the size of the neutron distribution in nuclei is given in sect. 6.

Finally a comparison can be made between the present results and the only other previous measurement by Abashian *et al.* [8]). At a momentum of 0.824 GeV/c for pions on lead, Abashian *et al.* obtained the ratio $\sigma_R^-/\sigma_R^+ = 1.050 \pm 0.011$, to be compared with the value 1.035 ± 0.009 obtained in the present work at 0.84 GeV/c from the absolute cross-section measurements. However, Abashian *et al.* made measurements over a restricted range of solid angles and used straight line extrapolations. If the present results are analysed in a similar way we obtain the value 1.049 ± 0.007 which is in good agreement with their data.

5. The pion-nucleus interaction

5.1. GENERAL CONSIDERATIONS

Our objective in this section is to show how the pion-nucleus interaction may be related to fundamental, known, quantities such as the pion-nucleon cross sections and

to the nuclear matter distribution which we wish particularly to study, and also how to use this interaction to make predictions for the quantity we have actually measured.

For intermediate energy nucleon-nucleus scattering there is a well-established sequence of arguments which allows us to make this connection. We assume that the nucleon-nucleus scattering can be described by a complex potential. The standard methods of potential scattering theory then yield the usual partial wave expressions for the reaction cross section and other observables in terms of reflection coefficients or phase shifts which can be determined by numerical integration of the Schrödinger equation with the given potential. The complex optical potential can be expressed via multiple scattering theory in terms of the nucleon-nucleon interaction in the nucleus and the impulse approximation can then be invoked to replace the two-nucleon interaction in the nucleus by the free two-nucleon interaction. This procedure makes it possible in principle to estimate the error in the use of impulse approximation and the corrections due to double scattering. It is also worth noting that the concept of an optical potential is used as a stage in the argument but it is not used in a phenomenological way as is customary in low and medium energy scattering, and that approximate solutions of the Schrödinger equation, e.g. the semi-classical approximation or Glauber theory, may be used when appropriate.

We intend to follow the same approach for the pion-nucleus interaction but there are a number of special features which arise when the projectile is a pion. Firstly, we note that because of the much smaller rest mass a pion with momentum of the order of 1 GeV/c is a relativistic particle; this means that we must use relativistic kinematics and must consider which wave equation is appropriate for the pion. Secondly, the pion-nucleon system goes through a number of resonances and in fact the large differences in the π^+p and π^-p total cross sections which are essential for the experiment arise when one system is in resonance and the other is not. Finally, the pion has the property that it may be totally annihilated in a collision with a single nucleon with high momentum in the nucleus or more usually with two nucleons of high relative momentum.

Neither the effect of resonances nor the effect of annihilation are formally taken into account in the high-energy multiple-scattering theory which we use to construct the optical potential. The usual prescription for estimating the effect of annihilation [ref. [18])] is to add to the free pion-nucleon cross section an effective cross section for absorption which is written as $\frac{1}{2}\Gamma\sigma_d$, where $\Gamma \approx 4$ and σ_d is the cross section for annihilation on a deuteron. In the energy range of our experiment, this effective cross section is of the order of 1 mb which represents a 2–3 % correction. This estimate of the correction is based on the assumption that the dependence of the absorption process on the nuclear matter distribution is the same as that for absorption in the optical model sense, i.e. removal from the elastic beam. However, it may be argued that because of the importance of the two-nucleon process the annihilation effect is more likely to depend on ρ^2 than on ρ and is therefore negligible in the nuclear surface region. A multiple-scattering theory for pion-nucleus scattering in the vicinity of the

(3, 3) resonance has recently been developed [19]). This uses a pion-nucleon interaction in the form of a resonance denominator and a separable numerator, with parameters chosen to fit the properties of the (3, 3) resonance. This interaction cannot readily be averaged over the momentum distribution of the nucleon in the nucleus and since this averaging process has a most important effect in the higher energy region, we have preferred to use the conventional multiple-scattering theory with Fermi-averaging as described in subsects. 5.3 and 5.5.

5.2. THE WAVE EQUATION

There are a number of relativistic wave equations which may be considered but there is no indisputably correct choice. Because we propose to construct the pion-nucleus potential from a multiple scattering theory based on the non-relativistic Lippman-Schwinger equation, we look for an equation which can be reduced to the form of the usual non-relativistic Schrödinger equation. This approach has obvious deficiencies, but we believe that it allows us to follow a consistent procedure fully analogous with that used at lower energies.

The relativistic Schrödinger equation for a particle moving in an external potential V is given by

$$[c(M_1^2c^2+p^2)^{\frac{1}{2}}+V]\psi = E_L\psi, \tag{5.1}$$

where E_L is the total energy of the particle in the laboratory system and M_1 is its rest mass. The Klein-Gordon equation is

$$[c^2p^2+M_1^2c^4]\psi = (E_L-V)^2\psi, \tag{5.2}$$

and these are shown by Goldberger and Watson [20]) to yield identical solutions when $|V| \ll M_1c^2$ and V changes slowly within one de Broglie wavelength. Eq. (5.2) may be rewritten as

$$[\nabla^2+k_L^2-u(r)]\psi = 0, \tag{5.3}$$

where

$$\hbar^2c^2k_L^2 = E_L^2-M_1^2c^4, \tag{5.4}$$

and

$$\hbar^2c^2u(r) = 2E_LV-V^2 \tag{5.5a}$$

$$\simeq 2E_LV, \tag{5.5b}$$

assuming $|V/E_L| \ll 1$ to obtain the last line. Thus eq. (5.3) with the approximation (5.5b) for the potential has the form of a non-relativistic Schrödinger equation and can be solved by the same techniques. The conditions for equivalence of eqs. (5.1) and (5.2) are also just those required for the validity of the semi-classical approximation which then gives a solution in the form

$$\psi = e^{i\boldsymbol{k}_L\cdot(\boldsymbol{b}+\hat{\boldsymbol{k}}_Lz)}e^{i\chi(b)}, \tag{5.6}$$

$$\chi(b) = \frac{-E_L}{\hbar^2c^2k_L}\int_{-\infty}^{\infty} V(\boldsymbol{b}+\hat{\boldsymbol{k}}_Lz)\,dz \tag{5.7a}$$

$$= \frac{-1}{\hbar v_L} \int_{-\infty}^{\infty} V(\boldsymbol{b} + \hat{\boldsymbol{k}}_L z)\,dz, \tag{5.7b}$$

where b is the impact parameter.

So far the discussion has been in terms of a particle of mass M_1 moving in an external potential V. We must now take account of the finite mass of the target nucleus. Following Goldberger and Watson [20]), then for the relativistic Schrödinger equation this can be done by adding a term $p^2/2M_2$ to the left-hand side of eq. (5.1) and also including the kinetic energy of the target in the total energy. This yields a Schrödinger-like equation of the form

$$[\nabla^2 + k^2 - u(r)]\psi = 0, \tag{5.8}$$

where, if E_1 and E_2 are the total energy of the pion and the target nucleus respectively in the pion-nucleus c.m. system, then

$$\hbar^2 c^2 k^2 = \frac{M_2 c^2}{E_1 + E_2} [(E_1 + E_2 - M_2 c^2)^2 - M_1^2 c^4], \tag{5.9}$$

$$\hbar^2 c^2 u(r) = 2DV(r), \tag{5.10}$$

$$D = \frac{M_2 c^2}{E_1 + E_2} (E_1 + E_2 - M_2 c^2). \tag{5.11}$$

In the limit of $M_2 \to \infty$ then $D \to E_L$ and $\hbar^2 c^2 k^2 \to E_L^2 - M_1^2 c^4$, so that eq. (5.8) then has the form (5.3) with the approximation (5.5b) for the potential. In the non-relativistic limit, $M_1 M_2 c^2/(E_1 + E_2) \to M_1 M_2/(M_1 + M_2)$ which is just the reduced mass μ, so that

$$k^2 \to \frac{2}{\hbar^2} \frac{M_1 M_2}{M_1 + M_2} \frac{M_2}{M_1 + M_2} T_L = \frac{2\mu}{\hbar^2} T_c,$$

$$u(r) \to \frac{2}{\hbar^2} \frac{M_1 M_2}{M_1 + M_2} V(r) = \frac{2\mu}{\hbar^2} V(r), \tag{5.12}$$

where T_L is the pion kinetic energy in the laboratory system and T_c its kinetic energy in the c.m. system. Eq. (5.8) then has the usual form of the non-relativistic Schrödinger equation.

For the Klein-Gordon equation there appears to be no corresponding procedure for taking into account the finite mass of the target nucleus. Some workers [21]) have simply used eq. (5.2) expressed in the form

$$[-\hbar^2 c^2 \nabla^2 + M_1^2 c^4]\psi = [E_L - V]^2 \psi,$$

or

$$[\nabla^2 + k_L^2 - (2E_L V - V^2)/\hbar^2 c^2]\psi = 0, \tag{5.13}$$

where E_L is the total energy of the incident pion in the laboratory system.

In the present work when deriving the potential V from the pion-nucleon interaction we have carefully carried out the appropriate transformations of the transition amplitude from the pion-nucleon c.m. system to the pion-nucleus c.m. system (see subsect. 5.3). We have therefore preferred also to use eq. (5.2) expressed in terms of c.m. quantities

$$[\nabla^2 + k_{\mathrm{c.m.}}^2 - (2E_1 V - V^2)/\hbar^2 c^2]\psi = 0, \tag{5.14}$$

where $k_{\mathrm{c.m.}}$ is the pion wave number and E_1 is its total energy in the pion-nucleus c.m. system (calculated using a Lorentz transformation). In the limit of a very heavy target nucleus this equation coincides with eq. (5.13). An alternative procedure often used for nucleon-nucleus scattering in the 150–200 MeV range [22]) is to write the Schrödinger equation in its usual non-relativistic form but to express the reduced mass in terms of the total energies in the c.m. system. This then gives

$$\left[\nabla^2 + k_{\mathrm{c.m.}}^2 - \frac{2E_1 E_2}{(E_1 + E_2)\hbar^2 c^2} V_{\mathrm{s}}\right]\psi = 0, \tag{5.15}$$

where $k_{\mathrm{c.m.}}$ is obtained from the Lorentz transformation. Comparing eqs. (5.15) and (5.14) it is concluded that they are identical if

$$V_{\mathrm{s}} = \frac{E_1 + E_2}{E_2} V \left(1 - \frac{V}{2E_1}\right).$$

As $V/2E_1$ is small for the pion-nucleus interaction over the energy region of interest in this work, we can write

$$V_{\mathrm{s}} \approx \frac{E_1 + E_2}{E_2} V. \tag{5.16}$$

For the momentum region of interest to this experiment we have confirmed that the solution of eq. (5.15) using (5.16) gives an excellent approximation to the exact solution of eq. (5.14). Both the exact and approximate method of solution were used in the present work.

We have made some numerical estimates of the effect on the calculated reaction cross sections and ratios for the momentum region of interest in this work, when using the various wave equations mentioned above. The relativistic Schrödinger equation (5.8)–(5.11) gives values about 2 % larger at 930 MeV/c and 4 % larger at 1850 MeV/c than eq. (5.14) for carbon. The effects for heavier nuclei are much smaller and the effect on the ratio of π^- to π^+ reaction cross sections for any nucleus is completely negligible.

A similar comparison of the results from solving the two forms of the Klein-Gordon equation (5.13) and (5.14) indicates that for carbon the difference in the calculated reaction cross sections is less than 0.3 %. For heavier nuclei the differences are expected to be much smaller and in all cases the effect on the π^-/π^+ ratio is negligible.

It may be concluded that despite the uncertainty about the wave equation to be

used both the relativistic Schrödinger equation and the Klein-Gordon equation used in either the laboratory or c.m. system give almost identical values for the reaction cross sections. All the results presented in the remainder of this paper were obtained using the Klein-Gordon equation in the form (5.14) and the form (5.15) with (5.16).

5.3. THE PION-NUCLEUS OPTICAL POTENTIAL

Following the multiple scattering theory of Watson [23]) the pion-nucleus optical potential may be expressed in terms of the pion-nucleon t-matrix. We define the pion-nucleon operator as

$$t_j = V_j + V_j Q G_0 t_j, \tag{5.17}$$

where Q is an operator which projects off the ground state of the target nucleus and G_0 is the propagator

$$G_0^{\pm} = (E - H_0 - H_N \pm i\varepsilon)^{-1} \tag{5.18}$$

with the nuclear Hamiltonian H_N and the kinetic energy operator H_0 for the pion. The multiple scattering series for the optical potential is then given by

$$\begin{aligned} U &= \langle 0|\tilde{U}|0\rangle \\ &= \langle 0|\sum_j t_j|0\rangle + \langle 0|\sum_{j\neq k} t_j Q G_0 t_k|0\rangle + \ldots, \end{aligned} \tag{5.19}$$

where $|0\rangle$ represents the ground state of the target nucleus. The first term of the expansion represents single pion-nucleon scattering summed to all orders and averaged over all the nucleons in the nucleus. The second term of this expansion represents double scattering, i.e. successive single scatterings from different nucleons, in which the intermediate states involve excited states of the nucleus. The exact scattering amplitude for elastic scattering is given in terms of the potential operator $\tilde{U}$ by

$$f(\boldsymbol{k}, \boldsymbol{k}') = -F\langle 0, \boldsymbol{k}'|\tilde{U} + \tilde{U}PG_0\tilde{U} + \ldots|0, \boldsymbol{k}\rangle, \tag{5.20}$$

where $P = 1 - Q$ and projects on to the nuclear ground state. The constant F is given by

$$F = E_1 E_2 / 2\pi\hbar^2 c^2 (E_1 + E_2) \tag{5.21a}$$

$$\rightarrow \frac{\mu}{2\pi\hbar^2} \text{(N.R. limit)}. \tag{5.21b}$$

Thus an exact solution of the Schrödinger equation with the potential U takes into account all multiple processes in which the intermediate states involve the ground state of the nucleus.

The first term in eq. (5.19) can be written in a momentum space representation as

$$U(\boldsymbol{k}, \boldsymbol{k}') = \sum_j \int \mathrm{d}\boldsymbol{p}_j \mathrm{d}\boldsymbol{p}_j' \delta(\boldsymbol{p}_j' + \boldsymbol{k}' - \boldsymbol{p}_j - \boldsymbol{k}) \langle \boldsymbol{p}_j', \boldsymbol{k}'|t_j|\boldsymbol{p}_j, \boldsymbol{k}\rangle \psi^*(\boldsymbol{p}_j')\psi(\boldsymbol{p}_j), \tag{5.22}$$

where $\boldsymbol{p}_j$, $\boldsymbol{p}_j'$ are the initial and final momenta of the struck nucleon. The nuclear momentum functions are defined as

$$\psi(\boldsymbol{p}_j) = \int \mathrm{d}\boldsymbol{r}_j \psi(\boldsymbol{r}_j) \mathrm{e}^{-i\boldsymbol{p}_j \cdot \boldsymbol{r}_j},$$

$$\psi^*(\boldsymbol{p}'_j) = \int \mathrm{d}\boldsymbol{r}'_j \psi^*(\boldsymbol{r}'_j) \mathrm{e}^{i\boldsymbol{p}'_j \cdot \boldsymbol{r}'_j},$$

where we suppress all but the jth position and momentum coordinate, and substituting those expressions into eq. (5.22) gives

$$U(\boldsymbol{k}, \boldsymbol{k}') = \sum_j \int \mathrm{d}\boldsymbol{p}_j \mathrm{d}\boldsymbol{r}_j \mathrm{d}\boldsymbol{r}'_j \langle \boldsymbol{p}_j + \boldsymbol{k} - \boldsymbol{k}', \boldsymbol{k}' | t_j | \boldsymbol{p}_j, \boldsymbol{k} \rangle \psi^*(\boldsymbol{r}'_j) \psi(\boldsymbol{r}_j) \mathrm{e}^{-i\boldsymbol{p}_j \cdot \boldsymbol{r}_t} \mathrm{e}^{i(\boldsymbol{p}_j + \boldsymbol{k} - \boldsymbol{k}') \cdot \boldsymbol{r}'_j}.$$

The standard procedure is now to replace the pion-nucleon scattering amplitude by an average value which depends on the momentum transfer and incident pion momentum so that it may be taken outside the integral. Integration over $\boldsymbol{p}_j$ then yields $\delta(\boldsymbol{r}_j - \boldsymbol{r}'_j)$ and integration over the space variables yields the nuclear form factor

$$F(q) = \int \rho(r) \mathrm{e}^{i\boldsymbol{q} \cdot \boldsymbol{r}} \mathrm{d}\boldsymbol{r}, \tag{5.23}$$

where $\rho(r)$ is the nuclear density distribution and q is the momentum transfer

$$\boldsymbol{q} = \boldsymbol{k} - \boldsymbol{k}'. \tag{5.24}$$

Finally,

$$U(q) = A \bar{t}_k(q) F(q) \tag{5.25}$$

and in coordinate space we obtain a local potential

$$U(r) = A \int \bar{t}_k(\boldsymbol{q}) F(q) \mathrm{e}^{-i\boldsymbol{q} \cdot \boldsymbol{r}} \mathrm{d}\boldsymbol{q}. \tag{5.26}$$

For the case when the pion-proton and pion-neutron scattering amplitudes are different, this must be written as

$$U^{\pm}(r) = Z \int \bar{t}_k^{\pm}(q) F_{\mathrm{p}}(q) \mathrm{e}^{-i\boldsymbol{q} \cdot \boldsymbol{r}} \mathrm{d}\boldsymbol{q} + N \int \bar{t}_k^{\mp}(q) F_{\mathrm{n}}(q) \mathrm{e}^{-i\boldsymbol{q} \cdot \boldsymbol{r}} \mathrm{d}\boldsymbol{q}, \tag{5.27}$$

where

$$F_{\mathrm{p}}(q) = \int \rho_{\mathrm{p}}(r) \mathrm{e}^{i\boldsymbol{q} \cdot \boldsymbol{r}} \mathrm{d}\boldsymbol{r}, \tag{5.28a}$$

$$F_{\mathrm{n}}(q) = \int \rho_{\mathrm{n}}(r) \mathrm{e}^{i\boldsymbol{q} \cdot \boldsymbol{r}} \mathrm{d}\boldsymbol{r}. \tag{5.28b}$$

In order to evaluate the potential in terms of known quantities we have to express the pion-nucleus t-matrix in the pion-nucleus c.m. system in terms of the pion-nucleon scattering amplitude in the pion-nucleon c.m. system. This has been done [24]) following the method of Kerman *et al.* [25]).

The resulting potential is

$$U^{\pm}(r) = \frac{-\hbar^2 c^2}{(2\pi)^2} \frac{W_1 + W_2}{E_1 \bar{E}_2} \int e^{-iq\cdot r} [Z f_k^{\pm}(q) F_p(q) + N f_k^{\mp}(q) F_n(q)] \, dq, \quad (5.29)$$

where W_1 and W_2 are the total energies of the pion and struck nucleon respectively in the pion-nucleon c.m. system, E_1 and $\bar{E}_2$ are the total energies for the same particles in the pion-nucleus c.m. system, and $\bar{E}_2 = E_2/A$. The scattering amplitudes $f_k^{\pm}(q)$ are in the pion-nucleon c.m. system.

Eq. (5.29) can be simplified if $f^{\pm}(q)$ varies slowly compared with $F(q)$, which is approximately true for heavy nuclei. The potential then becomes

$$U^{\pm}(r) = -2\pi\hbar^2 c^2 \frac{W_1 + W_2}{E_1 \bar{E}_2} [Z f_k^{\pm}(0) \rho_p(r) + N f_k^{\mp}(0) \rho_n(r)], \quad (5.30)$$

which involves only the forward scattering amplitudes. This formula has been frequently used in calculations on pion-nucleus scattering. However, since we are studying a range of nuclei, we have used both eqs. (5.29) and (5.30) and compared the results.

It is convenient to express the kinematical factor in the potential in terms of quantities defined in the laboratory system. Use of the appropriate Lorentz invariant quantities [25]) leads to the expression

$$\frac{W_1 + W_2}{E_1 \bar{E}_2} = \frac{\eta}{E_L} \frac{k_L}{k_0}, \quad (5.31)$$

where $\hbar k_L$, E_L are the pion momentum and total energy in the laboratory system, $\hbar k_0$ is the pion momentum in the pion-nucleon c.m. system and

$$\eta = 1 + \frac{M_2 c^2 E_L - M_2 c^2 M_1^2 c^4 / E_L}{M_2^2 c^4 + M_1^2 c^4 + M_2 c^2 E_L + M_2 c^2 M_1^2 c^4 / E_L}. \quad (5.32)$$

In the low-energy limit, η is close to unity while at high energies $\eta \to 2$.

5.4. THE PION-NUCLEON AMPLITUDES

The momentum dependence of the pion-nucleon scattering amplitude is usually expressed as [26])

$$f_k^{\pm}(q) = f_k^{\pm}(0) e^{-\frac{1}{4}\beta_{\pm}^2 q^2}. \quad (5.33)$$

This expression which appears to have some theoretical foundation [27]) also yields reasonable fits to pion-nucleon elastic scattering data not too far from the forward direction. Some examples of fits to the data are shown in fig. 7. We have determined values for $\beta_{\pm}^2$ by fitting such data and the values obtained are given in table 7.

The forward scattering amplitudes can be written in the form

$$f_k^{\pm}(0) = \frac{k_0}{4\pi} \sigma_T^{\pm}(i + \alpha^{\pm}), \quad (5.34)$$

where k_0 is the pion momentum in the pion-nucleon c.m. system and $\sigma_T^{\pm}$ are the total cross sections for $\pi^{\pm}$-p scattering. Values of $\sigma_T^{\pm}$ are taken from the work of Carter *et al.* [28]). The ratios $\alpha^{\pm}$ of the real to imaginary parts of the scattering amplitude are not well known but can be estimated from calculations using dispersion relations [29]).

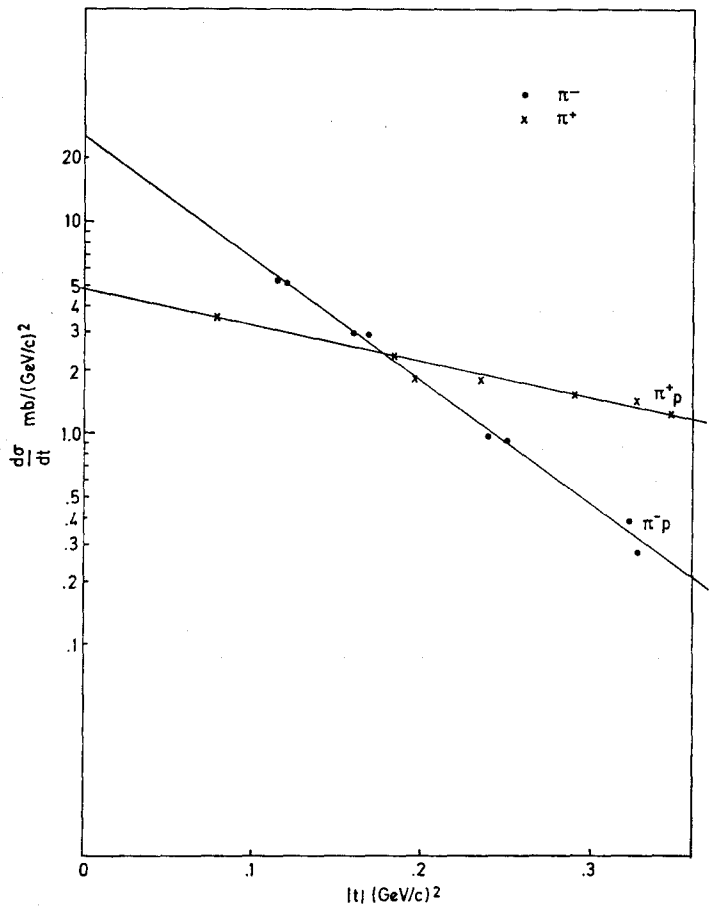

Fig. 7. Semi-logarithmic plot of the differential cross sections $d\sigma/dt$ for π^+ and π^- proton scattering at 1.00 GeV/c as a function of t. The straight lines represent best fits with expressions of the form $d\tau/dt = \sigma(0)e^{-\beta^2 t}$ where $t = q^2$.

TABLE 7

Values of β^2 obtained from fits to pion-nucleon scattering cross sections

Momentum (GeV/c)		0.71	0.84	1.00	1.36	1.58	2.00
π^+p	β_+^2	0.31	0.25	0.19	0.23	0.35	0.21
π^-p	β_-^2	0.29	0.27	0.47	0.33	0.29	0.31

The values of β^2 are in units of fm^2.

5.5. EFFECTS DUE TO FERMI MOTION

In subsect. 5.3 we assume that the pion-nucleon scattering amplitudes which appear inside the integral in eq. (5.22) could be replaced by a single averaged value. This procedure ignores the Fermi motion of the nucleons inside the nucleus and gives rise to an error in the evaluation of the potential. In the case of pion-nucleus scattering a more serious situation arises because of the resonance behaviour exhibited by the pion-nucleon total cross sections. This can be seen from fig. 1. The widths of those resonances are comparable to the range of Fermi momenta of the nucleons in the nucleus and therefore some improved treatment is necessary.

For zero momentum transfer, i.e. forward scattering, the integral in eq. (5.22) reduces to

$$\sum_j \int \mathrm{d}\boldsymbol{p}_j \langle \boldsymbol{p}_j | t_k(0) | \boldsymbol{p}_j \rangle |\psi(\boldsymbol{p}_j)|^2.$$

This suggests that an appropriate procedure is to average the forward scattering amplitude over the nuclear momentum distribution. This has been done for each laboratory pion momentum k_L by calculating the relativistic relative momentum k_R for a collision with a bound nucleon of momentum $\boldsymbol{p}$ and averaging the corresponding forward scattering amplitudes over the momentum distribution $\rho(\boldsymbol{p}) = |\psi(\boldsymbol{p})|^2$ so that the averaged amplitude is

$$\bar{f}_{k_L}(0) = \int f_{k_R}(0)\rho(\boldsymbol{p})\,\mathrm{d}\boldsymbol{p} \Big/ \int \rho(\boldsymbol{p})\,\mathrm{d}\boldsymbol{p}, \tag{5.35}$$

where k_R is a function of $\boldsymbol{p}$ for fixed k_L. This calculation was carried out separately for π^+ and π^- mesons on protons and on neutrons, and the averaging was done only with the imaginary parts of $f(0)$, i.e. the total cross sections.

The nuclear momentum distributions for protons and neutrons were obtained from several nuclear models. Calculations [24]) for ^{12}C, ^{40}Ca and ^{208}Pb were carried out using the single-particle model which gives

$$A\rho(\boldsymbol{p}) = \sum_\mu |\phi_\mu(\boldsymbol{p})|^2, \tag{5.36}$$

where the $\phi_\mu(\boldsymbol{p})$ are the Fourier transforms of the single-particle wave functions used to construct the proton and neutron distributions and hence to calculate the optical potential. This is obviously necessary to ensure consistency. Results were also obtained by Miller [17]) using the Fermi-gas model, where

$$\rho(p) \propto \frac{1}{1+\exp\left[(p-p_0)/\lambda\right]} \tag{5.37}$$

with $p_0 = 100$ MeV/c and $\lambda = 50$ MeV/c. The behaviour of these momentum distributions is shown in fig. 8. It turns out that the low momentum components dominate the averaging integral and that the distributions shown in the figure are sufficiently similar in this region to yield essentially identical results for the averaged am-

plitudes. This means that we have obtained a unique set of Fermi averaged $\pi^{\pm}$-p total cross sections. These are plotted in fig. 1 and the particular values associated with the pion momenta of our experiment are listed in table 8, where we have also given the ratios α of the real to imaginary part of the scattering amplitude.

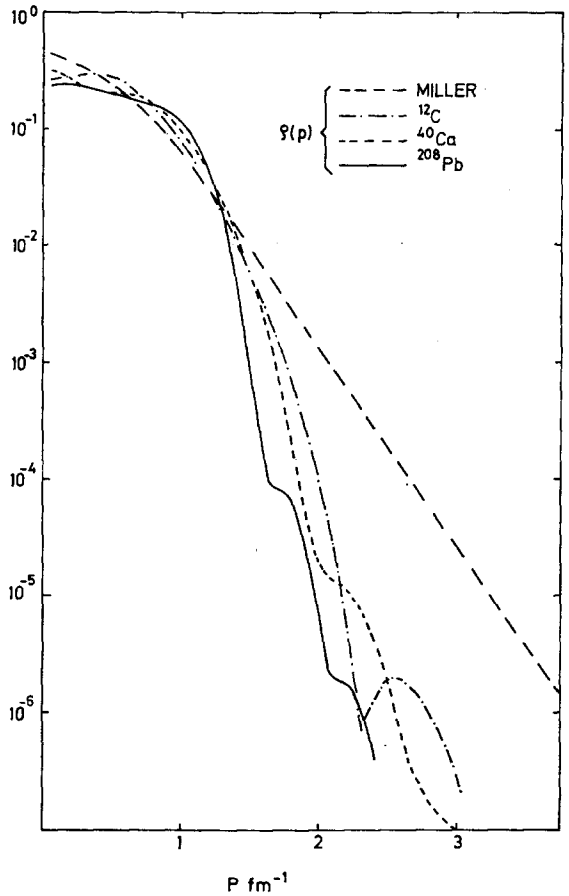

Fig. 8. Momentum distributions obtained using single-particle wave functions for ^{12}C, ^{40}Ca and ^{208}Pb. The distribution from the Fermi-gas model used by Miller [17]) is also shown.

TABLE 8

Fermi-averaged $\pi^{\pm}$-proton total cross sections and ratio of real to imaginary scattering amplitude

Momentum (GeV/c)	0.71	0.84	1.00	1.36	1.58	2.00
$\bar{\sigma}_T(\pi^+p)$ (mb)	17.11	19.76	25.71	37.63	36.12	30.50
$\bar{\sigma}_T(\pi^-p)$ (mb)	42.44	45.25	49.22	37.32	36.12	36.20
$\alpha(\pi^+p)$	−1.74	−0.90	−0.33	−0.06	−0.38	−0.36
$\alpha(\pi^-p)$	0.20	0.15	−0.04	−0.13	−0.14	−0.09

It can be seen from fig. 1 that an important effect of the averaging procedure is a dramatic reduction in the importance of the resonances. This effect has been noted before [12, 16]) and suggests that the theory has greater validity in the resonance region than might originally have been expected. It also shows that large errors will arise if the averaging procedure is not carried out, and this is confirmed by the results for free and averaged cross sections given in table 9.

TABLE 9

Values of σ_R and σ_R^-/σ_R^+ at 1.00 GeV/c obtained from the free and the Fermi-averaged pion-nucleon cross sections

Target	Pion-nucleon amplitude	σ_R^-	σ_R^+	σ_R^-/σ_R^+
^{12}C	free	270.8	268.5	1.009
	averaged	252.6	250.4	1.009
^{208}Pb	free	1806	1775	1.018
	averaged	1766	1724	1.024

5.6. SECOND-ORDER CORRECTIONS TO THE POTENTIAL

We have estimated the contribution arising from the second-order term in the multiple-scattering expansion (5.19) for the optical potential. This is of the form

$$\Delta U(k, k') = \langle 0|\sum_{j\neq k} t_j Q G_0 t_k|0\rangle$$
$$= \langle 0|\sum_{j\neq k} t_j G_0 t_k|0\rangle - \langle 0|\sum_{j\neq k} t_j P G_0 t_k|0\rangle. \tag{5.38}$$

Using closure, assuming that the excitation of the nuclear states is small, and assuming, as before, that the pion-nucleon amplitudes are functions of momentum transfer only, this can be written in configuration space as

$$\Delta U(\boldsymbol{r}, \boldsymbol{r}') = \frac{-\hbar^2}{2\mu} A(A-1)\int \frac{\mathrm{d}\boldsymbol{q}}{(2\pi)^3}\frac{\mathrm{d}\boldsymbol{q}'}{(2\pi)^3}[4\pi f(q')]\Delta(\boldsymbol{q}, \boldsymbol{q}')[4\pi f(-q)]$$
$$\times G(\boldsymbol{r}, \boldsymbol{r}')\mathrm{e}^{\mathrm{i}\boldsymbol{q}'\cdot\boldsymbol{r}}\mathrm{e}^{-\mathrm{i}\boldsymbol{q}\cdot\boldsymbol{r}'},$$

where $\Delta(\boldsymbol{q}, \boldsymbol{q}')$ is the Fourier transform of the two-nucleon density function and $f(q)$ is the pion-nucleon amplitude in the pion-nucleus c.m. system. Following Foldy and Walecka [30]), we now assume that the nuclear medium is uniform and use an eikonal approximation in order to obtain an expression for the propagator. We also take the two-nucleon density function to be of the form

$$\Delta(\boldsymbol{r}, \boldsymbol{r}') \approx \rho^2(r)\theta(|\boldsymbol{r}-\boldsymbol{r}'|) \tag{5.39}$$

and transform the pion-nucleon amplitude to the two-body c.m. system, as before. This yields a local second-order potential of the form

$$\Delta U(r) = \frac{-2i}{k} \frac{\hbar^2 c^2 (W_1 + W_2)^2 E_2}{E_1 \bar{E}_2 (E_1 + E_2)} A(A-1)\rho^2(r) \int_0^\infty q \, \mathrm{d}q \, \theta(q) \operatorname{arctg}(\lambda q) f_k^2(q), \quad (5.40)$$

where

$$\lambda = 2/A\rho(0)\sigma_T. \quad (5.41)$$

In the limit $\lambda \to \infty$ this expression for ΔU reduces to that given by Glauber [31]) which depends on the correlation length

$$C = \int_0^\infty \theta(x) \mathrm{d}x. \quad (5.42)$$

When the correction ΔU given by eq. (5.40) is added to the potential U given by eq. (5.29), the absolute values of the total reaction cross sections for ^{12}C are increased by about 1 % over the energy range spanned by this experiment.

Johnston and Watson [18]) write the two-nucleon density function in the form

$$\Delta(\boldsymbol{r}, \boldsymbol{r}') = \rho(\boldsymbol{r})[\rho(\boldsymbol{r}') + Q(\boldsymbol{R}, \boldsymbol{r}')], \quad (5.43)$$

where $\boldsymbol{R} = \boldsymbol{r} - \boldsymbol{r}'$, and set

$$\int_0^\infty Q \, \mathrm{d}\boldsymbol{R} = C/V_A, \quad (5.44)$$

where V_A is the nuclear volume. Here, C should be a function of $\boldsymbol{r}'$ but is treated as a constant, and this has the effect that ΔU becomes a function of $\rho(\boldsymbol{r})$ instead of $\rho^2(r)$. In the forward scattering approximation this gives

$$U + \Delta U \propto \left[\frac{A}{V_A} f(0) + i \frac{2\pi}{k} \frac{A}{V_A} f^2(0)\right] \rho(r). \quad (5.45)$$

This potential has been evaluated in the Fermi-gas model and yields an increase in the absolute values of the reaction cross section of 3 % for ^{12}C and 2 % for ^{208}Pb. This increase in the correction compared with the previous calculation is not surprising since the second-order potential now extends further into the surface region.

The small values of the corrections to σ_R which result from both calculations can be understood partly from the $1/k$ dependence of ΔU which decreases the importance of the correction at higher energies. In addition, in the formalism of Johnston and Watson [18]), the real part of the potential changes by 20 % while the imaginary part changes by 2 % and it is the imaginary part which essentially determines σ_R. Because of the many approximations made in these formulations of ΔU, the calculations yield only an indication of the corrections to the absolute values of σ_R, and very precise fits to these values would require a more careful treatment of the correlation function and the propagator, as has been done for nucleon-nucleus scattering by Kujawski [32]) and Johnson and Martin [33]). The important result which arises from our study is that, in both methods of calculation, the *ratios* of the reaction cross sections for π^+ and π^- mesons are changed by substantially less than 0.5 % for both light and heavy nuclei.

5.7. CALCULATIONS OF THE REACTION CROSS SECTIONS

We have calculated the reaction cross sections using the optical potentials defined by equations (5.29) and (5.30), together with the Fermi-averaged pion-nucleon amplitudes and various choices for the proton and neutron distributions in numerical or analytic form.

There are a number of possible ways of approaching the calculation, as discussed in subsect. 5.2. Given the potential $U(r)$, as derived in subsect. 5.3, we may insert the potential

$$V_s(r) = U(r) \tag{5.46}$$

into the Schrödinger equation (5.15). Alternatively the potential

$$V(r) = \frac{E_2\, U(r)}{E_1 + E_2} \tag{5.47}$$

may be used with the Klein-Gordon equation (5.14) or the same potential may be used in a Schrödinger equation whose total energy term includes the kinematic energy of the target [eqs. (5.8)–(5.11)]. In each case a Coulomb potential must be added to the nuclear potential.

Three different and independent computer programs have been used for the calculations:

(i) The program OPTAR developed by E. Friedman uses the potential $U(r)$ in eq. (5.15). Since the equation is in standard form and is linear in the nuclear and Coulomb potentials no special problems arise in this case.

(ii) A program for solving the Klein-Gordon equation based on eq. (5.14) has been developed at the University of Surrey. This includes terms linear and quadratic in the nuclear potential and linear in the Coulomb potential, and also includes V_C^2 for $Z < 68$.

(iii) The program ABACUS-M [ref. [34])] (kindly supplied by E. H. Auerbach) solves the Klein-Gordon equation (5.14) and includes V_C^2 but neglects V_N^2 and $V_N V_C$, where V_N and V_C are the nuclear and Coulomb potentials respectively. In addition, two programs using the semi-classical approximation were developed for test purposes, and for studies of the contribution of second-order terms in the potential.

Considerable efforts were made to obtain good agreement between the three programs. Very good agreement was found for the heavier targets, but discrepancies existed for the light nuclei. For 1 GeV/c pions incident on carbon, programs (i) and (ii) agreed to better than 0.3 % when the Coulomb potential was omitted but program (iii) deviated by 3 %. Further tests were then made by also setting the real part of the potential equal to zero and comparing the results with the reaction cross section calculated by the semi-classical approximation of Glauber [31]). Separate tests showed that at 1 GeV/c this method gives the correct σ_R to better than 0.3 %. It was found that the semi-classical results agreed with programs (i) and (ii). A careful study of ABACUS-M then suggested that there have been two approximations which were

not very accurate for light nuclei and for momenta of about 1 GeV/c and above. These approximations were in the transformation from laboratory to c.m. system and in the expression for the potential in the radial equation. When this had been rectified, the agreement between programs (i) and (iii) was better than 0.1 % over the whole range. When the Coulomb potential was included in the calculations it was still found that programs (i) and (iii) agreed to better than 0.1 % for all nuclei and all momenta. This independence of σ_R on the V_C^2 term in the Klein-Gordon equation for the present range of nuclei and momenta can easily be understood since $V_C/2E_1$ is of the order of 1 % or less for all cases [see eq. (5.16)]. Programs (ii) and (iii) agree to within 0.3 % for all nuclei over the range of pion momenta covered in this experiment.

In the programs OPTAR and ABACUS-M, the calculation of two Fourier transforms, one to obtain the form factor and the other to obtain the potential, was avoided by noting that [3])

$$\frac{1}{2\pi}\int e^{-i\boldsymbol{q}\cdot\boldsymbol{r}} e^{-\frac{1}{4}\beta^2 q^2} F(q)\,d\boldsymbol{q} = \frac{2\pi}{\pi^{\frac{3}{2}} a_g^3}\int \exp\left(-|\boldsymbol{r}-\boldsymbol{r}'|^2/ag^2\right)\rho(r')\,d\boldsymbol{r}' , \qquad (5.48)$$

where $a_g^2 = 2\beta^2$. The Gaussian function looks like an effective interaction but it is used here for mathematical convenience and no physical significance should be attached to it as an effective pion-nucleon interaction. The Gaussian folding was carried out separately for the proton and neutron density terms in the potential.

6. Nuclear density distributions

In this section we present a detailed analysis and interpretation of the experimental results in terms of nuclear density distributions. The main emphasis is on an analysis of the ratios σ_R^-/σ_R^+ of the π^--nucleus to π^+-nucleus reaction cross sections, in order to obtain information on the difference between the proton and the neutron distributions. A comparison is also made between the measurements and theoretical predictions for the absolute values of σ_R^- and σ_R^+.

For each target nucleus we have at most two pieces of experimental data, σ_R^- and σ_R^+, at a given incident pion momentum. If we concentrate on the ratios σ_R^-/σ_R^+ in order to take advantage of some cancellation of experimental errors and uncertainties in the theory, we have only one data point at each pion momentum. We cannot expect, therefore, to determine a unique set of parameters for each nuclear density distribution. Instead, we endeavour to establish what range of parameters is acceptable and which nuclear models are consistent with our data. As will be seen later, we are indeed able to exclude certain models which have hitherto found favour.

6.1. LOCALIZATION OF THE PION ABSORPTION

It is of interest to investigate what region of the nucleus this experiment has probed and to indicate to what extent this changes with incident pion momentum. We have

done this by several methods, two of which are based on the semi-classical approximation for the reaction cross section. This approximation gives

$$\sigma_R^{\pm} = 2\pi \int_0^{\infty} \{1 - \exp[-2 \operatorname{Im} \chi^{\pm}(b)]\} b \, db, \tag{6.1}$$

where $\chi(b)$ is given by eq. (5.7a). Substituting from eqs. (5.30) and (5.31) into eq. (5.7a) and using the optical theorem, we obtain

$$2 \operatorname{Im} \chi^{\pm}(b) = \int_{-\infty}^{\infty} [\sigma^{\pm} Z \rho_p(r) + \sigma^{\mp} N \rho_n(r)] \, dz. \tag{6.2}$$

The integrand $I_1(b)$ from eq. (6.1), i.e.

$$I_1^{\pm}(b) = \{1 - \exp[-2 \operatorname{Im} \chi^{\pm}(b)]\} b,$$

has been plotted for π^+ and π^- mesons on Pb, and typical curves are shown in fig. 9. The proton and neutron distributions were taken to be Fermi distributions with parameters $R_p = R_n = 6.66$ fm and $a_p = a_n = 0.45$ fm. It can be seen that the integrands peak at about 6 fm for both π^- and π^+ scattering but the difference between the two integrands peaks at about 7 fm. The behaviour at other energies is very similar except that the magnitude of the difference term varies.

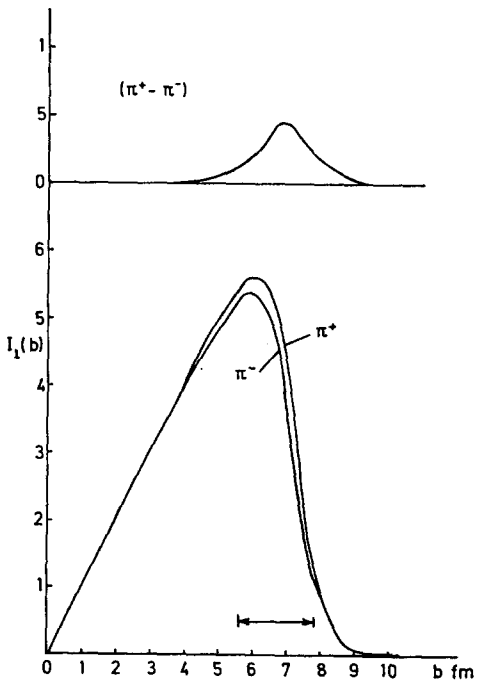

Fig. 9. The integrand $I_1(b)$ of eq. (6.1) for π^- and π^+ mesons on lead at 710 MeV/c. The upper curve gives the difference between the integrands for π^- and π^+ mesons. For parameters see subsect. 6.1.

An alternative way of investigating where the pion absorption occurs is to consider summed inelastic and quasi-elastic scattering. (It should be stressed that we mean absorption in the optical model sense, i.e. removal from the elastic beam, and not annihilation of the pion.) This leads to an expression [35]) for the pion-nucleus cross section in which the leading term is a product of the free pion-nucleon cross section and the effective nucleon number $N(A)$ which is given by

$$N(A) = \int A\rho_m(r) \exp\left[-2 \operatorname{Im} \chi(b)\right] \mathrm{d}r \tag{6.4a}$$

$$= 2\pi \int I_2(b)\, \mathrm{d}b \tag{6.4b}$$

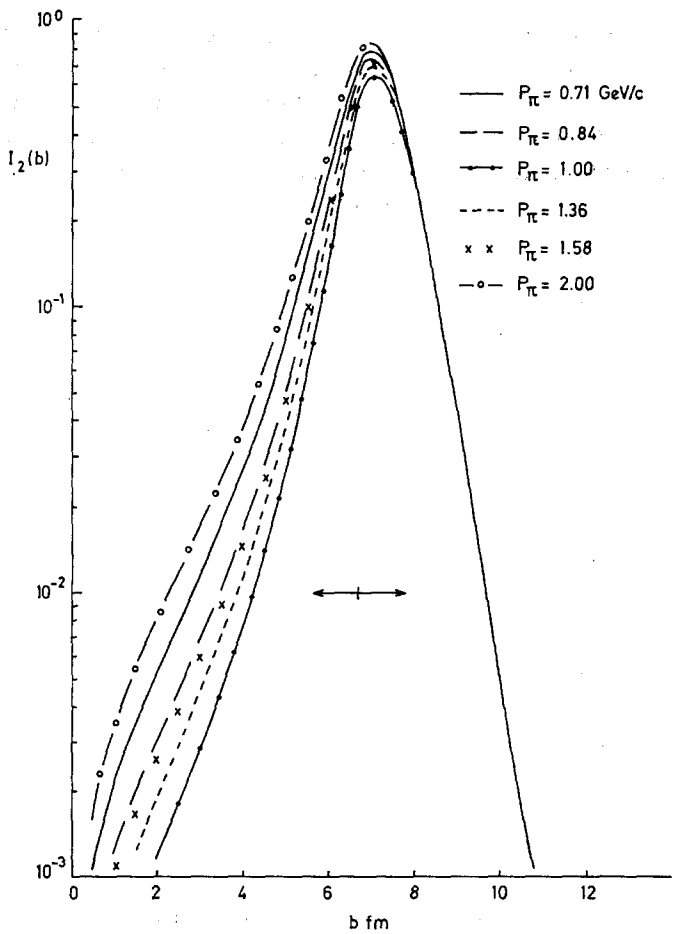

Fig. 10. The integrand $I_2(b)$ of eq. (6.4b) for π^+ scattering from lead at the momenta used in this experiment. For parameters and discussion see subsect. 6.1.

with

$$I_2(b) = b \exp\left[-2 \operatorname{Im} \chi(b)\right] \int_{-\infty}^{\infty} A\rho_m(r)\,dz. \tag{6.5}$$

This integrand has been plotted in fig. 10 for π^+ scattering from Pb, again using Fermi distributions with $R_p = R_n = 6.66$ fm and $a_p = a_n = 0.45$ fm. It can be seen that the integrand I_2 is localized in the same region of the nucleus but at a slightly larger radius than I_1. The region of localization is not strongly dependent on pion momentum, although it does depend on p_π in a manner which reflects the behaviour of the pion-nucleon cross sections. Variations in the parameters of the neutron distribution over a reasonable range do not change the curves very much.

We may conclude from these studies that, for the range of pion momentum used in this experiment, the processes which contribute to the removal of pions from the elastic beam and hence give rise to the measured reaction cross section occur mainly in the transition region of the nucleus, i.e. the 90 %–10 % density region, which has been indicated by arrows on figs. 9 and 10. It is this region which essentially determines the values of radial parameters such as the mean square radius and which for the proton distribution is well-determined by electromagnetic measurements. There is no sensitivity at all to the interior region and slight sensitivity to the region where the density is less than 10 % of the average central value.

6.2. CHOICE OF DENSITY DISTRIBUTIONS

We have chosen to use, as far as possible, density distributions which have been derived by fitting other data, such as electron scattering, separation energies, and Coulomb energy differences.

For ^{12}C, harmonic oscillator functions can be used to construct a proton density distribution (HO) which fits the electron scattering data for momentum transfers up to ≈ 2.5 fm^{-1}. The neutron distribution has been taken to be the same as the proton distribution. The Elton-Swift distributions (ES) have been constructed [36]) from single-particle wave functions generated in Saxon-Woods potentials by requiring reasonable agreement with the observed separation energies and good fits to the electron scattering data. The r.m.s. radii of these distributions are listed in table 10.

For ^{40}Ca, we have used the Batty-Greenlees (BG) distributions [6]) which have also been generated in Saxon-Woods potentials by requiring good agreement with the energies of single-particle and single-hole states near to the Fermi surface. The proton distribution also fits the electron scattering data up to medium values of momentum transfer. An additional neutron distribution has been generated by putting the neutrons in the BG potential for protons and adjusting the depth to give the correct separation energy for the last neutron. This distribution is labelled (P) and it can be seen from table 10 that it leads to a neutron distribution with a smaller r.m.s. radius than the proton distribution.

For nickel, tin and lead, we have used phenomenological Fermi distributions (F),

TABLE 10
Parameters of nuclear density distributions

		Refs.	$\langle r^2\rangle_p^{\frac{1}{2}}$	$\langle r^2\rangle_n^{\frac{1}{2}}$	$\langle r^2\rangle_n^{\frac{1}{2}} - \langle r^2\rangle_p^{\frac{1}{2}}$
^{12}C	HO	[43])	2.45	2.45	0
	ES	[36])	2.46	2.43	−0.03
^{40}Ca	BG	[6])	3.41	3.45	0.04
	P		3.41	3.31	−0.10
Ni	F		3.84	3.84	0
Sn	F		4.53	4.53	0
^{208}Pb	BG	[6])	5.44	6.06	0.62
	ZD	[37])	5.44	5.43	−0.01
	NEG	[7])	5.37	5.60	0.23
	HYD	[38])	5.44	5.39	−0.05
	F		5.42	5.42	0

and in general have taken $\langle r^2\rangle_n^{\frac{1}{2}} = \langle r^2\rangle_p^{\frac{1}{2}}$. Typical parameters are listed in table 10. We have also used, for ^{208}Pb, a variety of distributions which have recently appeared in the literature. Distribution NEG arises from the Hartree-Fock calculations by Negele [7]) and yields reasonable agreement with electron scattering data, the ZD distribution has the same proton distribution as in the BG model but has a neutron distribution calculated from the single-particle potential of Zaidi and Darmodjo [37]) which leads to better agreement with data from neutron transfer reactions, and the HYD density distribution comes from a calculation using the hydrodynamical model [ref. [38])]. The r.m.s. radii of these distributions are listed in table 10.

There is an important difference between the HO distribution and the other single-particle distributions, which must be taken into account in our calculations. Because of the analytic form of the oscillator functions it is possible to apply a correction for c.m. motion in the shell-model potential. This is done when fitting electron scattering data and therefore must also be done when calculating the optical potential with this distribution. The other single-particle distributions are obtained by numerical integration of the Schrödinger equation with a Saxon-Woods potential. In some cases comparison with electron scattering has been done using a c.m. correction derived from the oscillator model [7]). If no correction has been applied for electron scattering calculations, it should not be applied when these distributions are used for other calculations. In the present calculations this correction has been applied when appropriate.

6.3. ANALYSIS OF σ_R^-/σ_R^+

6.3.1. Results at 1.36 and 1.58 GeV/c. We have already stressed that the calculated ratios are almost independent of corrections to the first order optical potential. The estimated changes in the ratios due to addition of the second order term in the potential are substantially less than 0.5 % (see subsect. 5.6). The largest change in a ratio observed when the momentum dependence of the pion-nucleon amplitude is taken into account (see subsect. 5.4) is 1 %. Therefore an important test of the method is

given by the results at 1.36 and 1.58 GeV/c since at these momenta the Fermi-averaged π^+-p and π^--p total cross sections are equal. It follows from eq. (5.29) that the imaginary parts of the nuclear potentials for π^+ and π^- scattering are identical and the only difference in the scattering arises from the opposite signs of the Coulomb potentials and a very small effect due to the slightly different real nuclear potentials.

A comparison of theoretical and experimental results at 1.36 and 1.58 GeV/c is given in table 11. Excellent agreement is obtained which serves to confirm the validity of the method and the accuracy of the calculations. The departure of these ratios from unity illustrates the importance of Coulomb effects. It is clear that a semi-classical calculation or any other method which does not treat Coulomb scattering correctly will not lead to reliable results.

TABLE 11

Experimental and theoretical values for the σ_R^-/σ_R^+ ratio at 1.36 and 1.58 GeV/c

Target	C	Al	Ca	Ni	Sn	Ho	Pb
1.36 GeV/c							
exp.	1.007±0.007	1.014±0.009	1.015±0.007	1.027±0.005	1.030±0.005	1.041±0.009	1.043±0.007
theor.	1.006	1.012	1.016	1.021	1.032	1.038	1.043
1.58 GeV/c							
exp.	1.006±0.009	1.013±0.008	1.015±0.008	1.020±0.006	1.029±0.006		1.039±0.006
theor.	1.005	1.010	1.014	1.018	1.027		1.038

6.3.2. Results for carbon. The experimental and theoretical results for this nucleus are shown in fig. 11. The ES distribution yields somewhat better agreement with the data than the HO distribution which has $\langle r^2\rangle_p^{\frac{1}{2}} = \langle r^2\rangle_p^{\frac{1}{2}}$. However, calculations with an HO distribution with parameters modified to give the same r.m.s. radii as the ES distribution give almost identical results to that model. Thus it appears that the data are basically sensitive to the difference between the proton and neutron distributions, as reflected by the difference in r.m.s. radii, and can be used to detect a difference in excess of 0.07 fm in ^{12}C.

6.3.3. Results for calcium. The results for calcium are also shown in fig. 11. The nucleus ^{40}Ca accounts for 97 % of the natural calcium target and we have used different proton and neutron distributions for this nucleus in analysing the data. Since the two curves correspond to the same proton distribution it is evident the experiment is sensitive to the difference in the two neutron distributions and that the one with $\langle r^2\rangle_n^{\frac{1}{2}} - \langle r^2\rangle_p^{\frac{1}{2}} \approx -0.1$ fm is preferred. This is consistent with the results of Hartree-Fock and Thomas-Fermi calculations for this nucleus [7, 39]).

6.3.4. Results for lead. Measurements have been carried out for a natural lead target and for a target of separated ^{208}Pb. From the experimental results given in subsect. 4.4 it can be seen that no significant difference between the two has been observed. Some calculations have been carried out for ^{206}Pb but the results are iden-

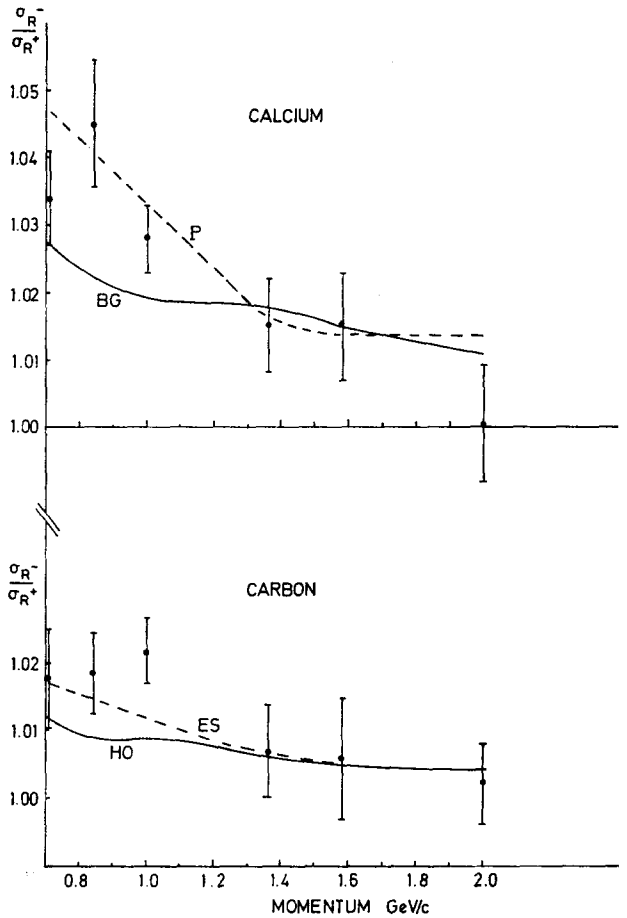

Fig. 11. Measured ratios σ_R^-/σ_R^+ as a function of incident momentum for carbon and calcium. The curves show the theoretical predictions for different nuclear density distributions (see subsects. 6.2, 6.3.2 and 6.3.3).

tical with those obtained for ^{208}Pb. For these reasons we compare calculations for ^{208}Pb with the more accurate experimental data obtained for the natural Pb target.

In fig. 12 we compare the experimental results with values predicted by the distributions described in subsect. 6.2. By comparison with table 10 it is clear that those models which predict a large difference between the neutron and proton r.m.s. radii do not yield acceptable agreement with the data. When several types of distribution are used, the difference between the r.m.s. radii of the proton and neutron distribution does not uniquely determine the ratio σ_R^-/σ_R^+ and there is clearly some dependence on the details of the distribution. However, this dependence is not strong and it can be concluded from fig. 12 that $\langle r^2\rangle_n^{\frac{1}{2}} - \langle r^2\rangle_p^{\frac{1}{2}} = 0.0 \pm 0.1$ fm, with perhaps a slight preference for a negative value. The results for Pb have also been compared with calculations in which the parameters of the neutron distribution were varied systemati-

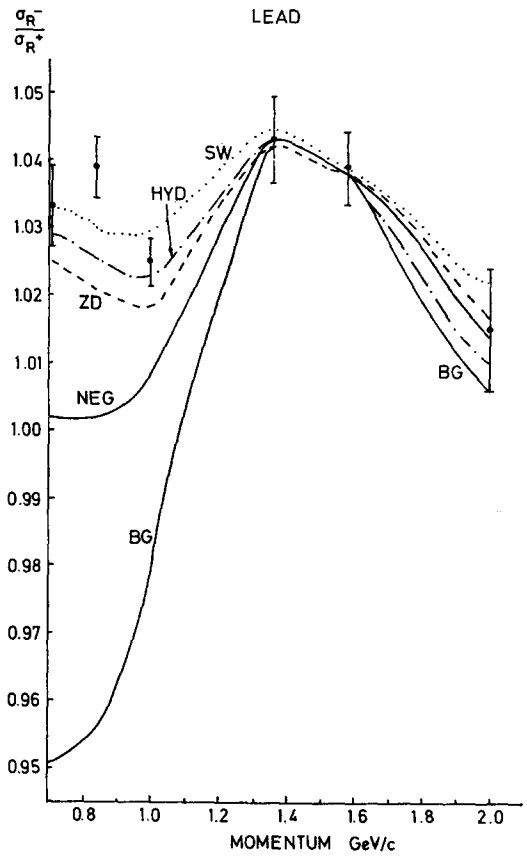

Fig. 12. Measured ratios σ_R^-/σ_R^+ as a function of incident momentum for lead. The curves show the theoretical predictions for different nuclear density distributions (see subsects. 6.2 and 6.3.4).

cally. Both proton and neutron distributions were assumed to be of Fermi shape and the parameters for the protons were fixed at the values (R_p = 6.66 fm and a_p = 0.45 fm) obtained from analyses of electron scattering data. Following the analysis presented in the earlier paper [40]) on this experiment the parameters for the neutron distribution were varied in steps of 0.1 fm over the range R_n = 6.4 to 7.2 fm and a_n = 0.3 to 0.9 fm. However, in contrast to the previous analysis the full optical potential [eq. (5.29)] including the momentum transfer dependence of the pion-nucleon scattering amplitudes was used. The results of these calculations for lead at a momentum of 0.84 GeV/c are shown in fig. 13a. It is seen that a range of R_n and a_n values from R_n = 6.4 fm and a_n = 0.49 fm to R_n = 6.93 fm and a_n = 0.3 fm would give good fits to the experimental ratio. In fig. 13(b) we have plotted the results of the same calculations of the ratio and covering the same R_n and a_n values as in the previous figure but this time as a function of the r.m.s. radius of the neutron distribution. It is seen that for a given type of distribution, the r.m.s. radius is a quantity which is quite well

defined by a measurement of the ratio of π^-/π^+ reaction cross sections. If the curves in fig. 13b fell on top of each other, the r.m.s. radii would of course be precisely determined, within this particular model. The value obtained from fig. 13b is 5.38 ± 0.10 fm for the r.m.s. radius of the neutron distribution. Similar analyses at 0.71 and 1.00 GeV/c give values of 5.44 ± 0.10 and 5.44 ± 0.11 fm giving a mean for all three values of 5.42 ± 0.06 fm. This result is to be compared with the value used in this calculation of 5.42 fm for the proton distribution.

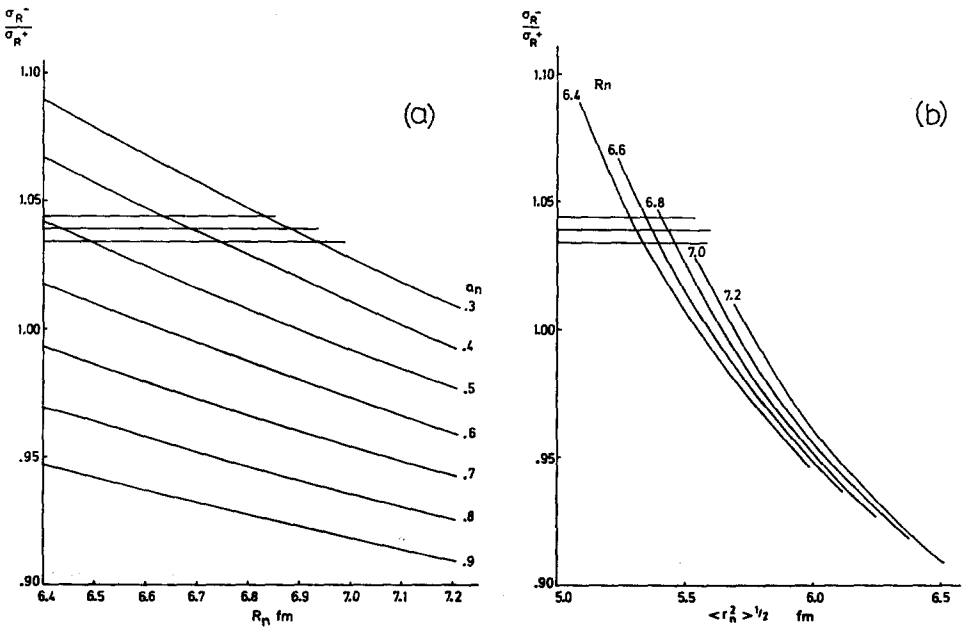

Fig. 13. (a) The ratio σ_R^-/σ_R^+ for lead at 0.84 GeV/c predicted using a Fermi neutron distribution and a range of R_n and a_n values. (b) The ratio, as in (a), but plotted as a function of the r.m.s. radius of the neutron distribution.

6.3.5. Results for other nuclei. Similar though less detailed calculations have been made for the other nuclei studied. Fig. 14 shows comparisons between experimental and theoretical values of the ratio for nickel and tin. As in the case of lead, the calculated ratios do not vary significantly for different isotopes of the same element, and the curves shown in fig. 14 correspond to atomic weights appropriate to the natural mixture of isotopes. The same Fermi distribution was assumed for the proton and neutron distributions, so that $\langle r^2 \rangle_n^{\frac{1}{2}} = \langle r^2 \rangle_p^{\frac{1}{2}}$. Calculations using density distributions derived from the hydrodynamical model [38]), for which $\langle r^2 \rangle_n^{\frac{1}{2}} - \langle r^2 \rangle_p^{\frac{1}{2}} \approx -0.04$ fm for nickel and tin, gave results indistinguishable from those plotted in the figure. The agreement with the data is very satisfactory for tin and reasonably so for nickel.

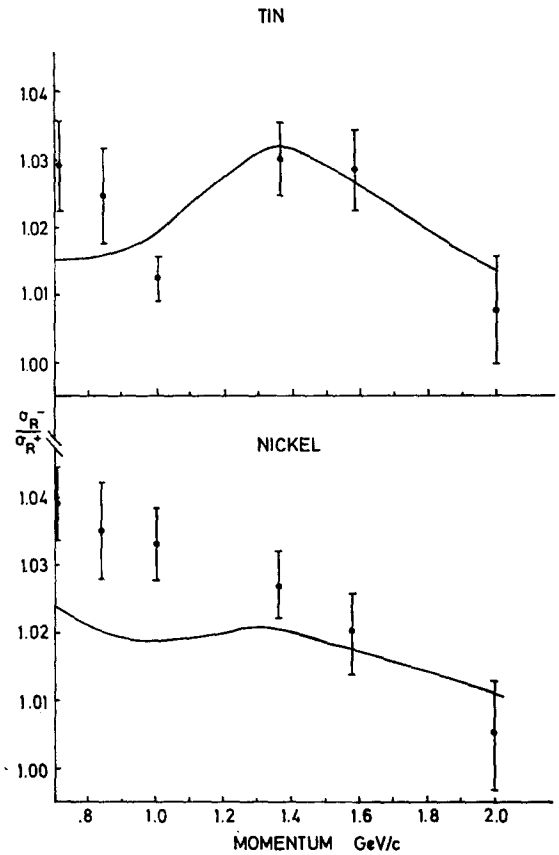

Fig. 14. Measured ratios σ_R^-/σ_R^+ as a function of incident momentum for nickel and tin. The curves show the theoretical predictions assuming the parameters of the neutron and proton distributions are the same.

6.4. ANALYSIS OF THE ABSOLUTE VALUES OF σ_R

We have shown that the ratios of the cross sections are insensitive to uncertainties in the calculation, but a gross failure of the theory to predict the absolute values would nevertheless cast considerable doubt on the reliability of the interpretation of the results given in the previous section. On the other hand agreement between the predicted and measured cross sections would give confidence in the interpretation of the ratio values in terms of nuclear sizes.

6.4.1. Results at 1.36 and 1.58 GeV/c. The absolute values are sensitive both to the validity of the treatment of the pion-nucleus interaction and to the choice of proton and neutron distributions.

For pion momenta of 1.36 and 1.58 GeV/c the Fermi-averaged π^+-p and π^--p cross sections are identical, and this means that the values of σ_R depend on the matter distribution but not on the difference between the proton and neutron distributions.

Results for ^{12}C, ^{40}Ca and ^{208}Pb at 1.36 GeV/c are listed in table 12. It can be seen that inclusion of the momentum transfer dependence of the pion-nucleon scattering amplitude increases the calculated values by 7 % and 4 % for ^{12}C and ^{208}Pb respectively and that it considerably improves the agreement with experiment. The effect of the β^2 dependence on the optical potential for ^{12}C is shown in fig. 15. (It can be seen from this figure that $|V|/M_\pi c^2 \lesssim 0.4$. This means that the criterion for equivalence of the Klein-Gordon and Schrödinger equations is moderately, but not well,

TABLE 12

Calculated and experimental values for π-nucleus reaction cross sections at 1.36 GeV/c

Projectile	Target	Density distribution	σ_R(mb)			
			no momentum dependence	momentum dependence	momentum dependence + second order	exp.
π^+	^{12}C	HO	227.8	243.6	251.4	248 ± 3
π^+	^{12}C	ES	231.9	247.4		248 ± 3
π^-	^{12}C	HO	229.4	245.1	253.0	254 ± 2
π^-	^{12}C	ES	233.5	249.0		254 ± 2
π^+	^{40}Ca	P	556.5	581.5		599 ± 4
π^-	^{40}Ca	P	566.0	591.0		611 ± 4
π^+	^{208}Pb	ZD	1680	1751	1779	1743 ± 13
π^+	^{208}Pb	NEG	1699	1751	1779	1743 ± 13
π^-	^{208}Pb	ZD	1757	1825	1856	1817 ± 9
π^-	^{208}Pb	NEG	1777	1827	1858	1817 ± 9

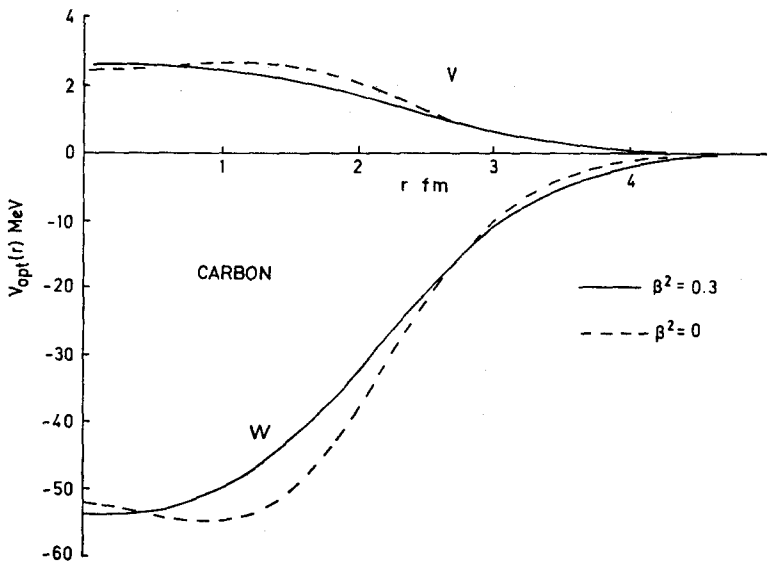

Fig. 15. The calculated optical potential for carbon at 0.84 GeV/c showing the effect of including the momentum dependence of the pion-nucleon scattering amplitudes ($\beta^2 = 0.3$).

satisfied.) The second-order corrections have been calculated using the Johnston and Watson method (see subsect. 5.6) and this probably overestimates the corrections. Omitting the second-order correction but including the momentum dependence of the pion-nucleon amplitudes, the differences between theory and experiment are less than 4 % for ^{12}C, less than 3 % for ^{40}Ca, and less than 1 % for ^{208}Pb. This is quite remarkable considering that there are no adjustable parameters in the theory.

The agreement between the predictions obtained from the various models for the density distributions suggests that these models give a generally correct description of the nuclear matter distribution. For example, for ^{208}Pb the ZD distributions give $\langle r^2\rangle_{\mathrm{m}}^{\frac{1}{2}} = 5.49$ fm whereas Negele's distributions give $\langle r^2\rangle_{\mathrm{m}}^{\frac{1}{2}} = 5.51$ fm and it is therefore not surprising that they predict the same absolute values at these pion momenta. Negele's value for $\langle r^2\rangle_{\mathrm{p}}^{\frac{1}{2}}$ is slightly below the value deduced from other experiments and the difference $\langle r^2\rangle_{\mathrm{n}}^{\frac{1}{2}} - \langle r^2\rangle_{\mathrm{p}}^{\frac{1}{2}}$ is somewhat too big to give agreement with $\sigma_{\mathrm{R}}^{-}/\sigma_{\mathrm{R}}^{+}$. The hydrodynamical model predicts cross sections which are about 2 % smaller than those predicted from the ZD and Negele's distributions; this is consistent with the theoretical values for ^{12}C and ^{40}Ca which are about 3 % below the experimental ones, and we could expect the discrepancy to be made up by the second-order contribution to the potential.

6.4.2. Results at 2.00 GeV/c. A comparison of theoretical and experimental results for π^- mesons on ^{12}C, ^{40}Ca and ^{208}Pb is shown in fig. 16. For both π^+ and π^- scattering from all targets, the calculated values of σ_{R} are about 3 % above the experimental values at 2.00 GeV/c. It is difficult to attribute this to any systematic error in the experiment because the pion-hydrogen total cross sections have been measured during the same experiment, by the CH_2-C difference method, and were found to be in agreement with the published values. At this momentum, we are well beyond the main pion-nucleon resonance region; the validity of theory should be particularly good and the magnitude of the corrections should be small. Apart from the speculation that the sign of the multiple-scattering correction could be reversed, we are unable to offer an explanation for the sign reversal in the difference between theory and experiment at this pion momentum.

6.4.3. Results at 0.71, 0.84 and 1.00 GeV/c. The three lowest pion momenta are in the region where there are fairly large resonances in the pion-nucleon system, and therefore more difficulties in obtaining agreement with the absolute values might be expected. The agreement between theory and experiment is, in fact, as good at 1.00 GeV/c as it is at 1.36 and 1.58 GeV/c, except perhaps for ^{12}C. Only at 0.71 and 0.84 GeV/c do the differences approach 10 %.

We have tried to improve the agreement at the two lowest momenta by some adjustments in the parameters, particularly the π^--p cross section since it is this system which is in resonance. It turns out, however, that no simultaneous agreement for the absolute values and the ratios could be obtained unless the smooth π^+-p cross sections were adjusted by a larger amount than the resonating π^--p cross sections or unreasonable neutron distributions were assumed such that $\langle r^2\rangle_{\mathrm{n}}^{\frac{1}{2}} - \langle r^2\rangle_{\mathrm{p}}^{\frac{1}{2}} \approx -0.5$ fm. This

suggests that the Fermi-averaging procedure deals sufficiently with the resonant effects and that no further modification of the first-order term in the potential is called for.

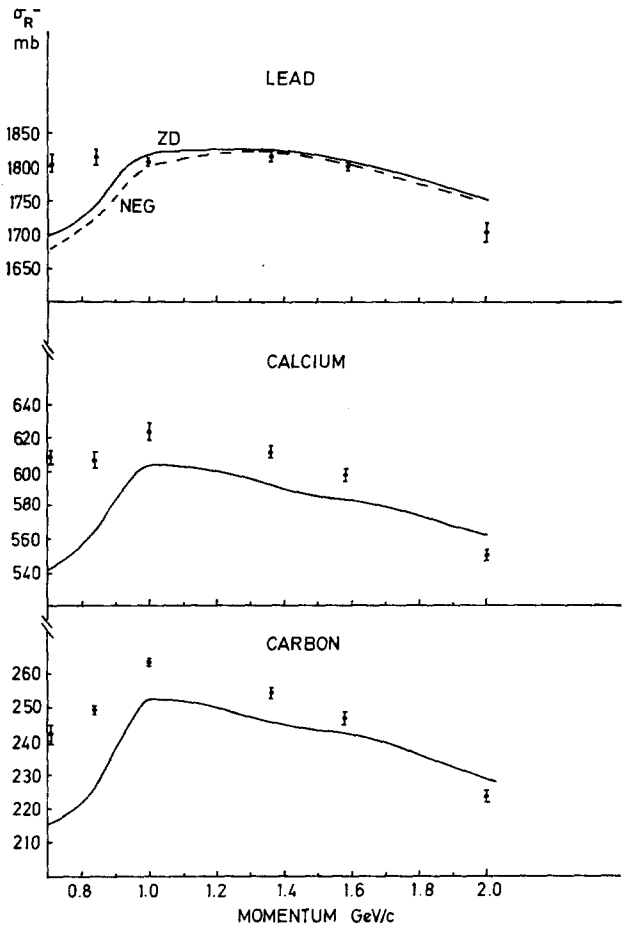

Fig. 16. Comparison of experimental and predicted reaction cross sections for π^- mesons on ^{12}C, ^{40}Ca and ^{208}Pb as a function of momentum.

6.5. COMPARISON WITH OTHER EXPERIMENTAL METHODS

In this section we review briefly the results regarding neutron density distributions obtained by other experimental methods and compare them with the conclusions reached in the present experiment. A more detailed comparison may be found elsewhere [41]).

The microscopic approach to the nucleon-nucleus optical potential by Greenlees *et al.* [1]) has been used to derive information on the neutron density distribution, and in particular on its r.m.s. radius. For ^{208}Pb they find that the difference between the neutron and proton r.m.s. radii is approximately 0.2 fm with an uncertainty of at least

± 0.1 fm. This is not inconsistent with the present results. For medium-weight nuclei they generally obtain no difference. However the results are rather sensitive to the choice of the effective interaction.

Another method of studying neutron distributions in nuclei is the analysis of the elastic scattering of alpha particles using the microscopic approach [2]). This method seems to be most suitable for analysing the elastic scattering of alpha particles below the Coulomb barrier, and the analysis by Batty and Friedman [2]) showed that the ZD density distribution leads to agreement between theory and experiment for Pb isotopes, whereas if $\langle r^2\rangle_n^{\frac{1}{2}} - \langle r^2\rangle_p^{\frac{1}{2}} = 0.6$ fm no agreement can be achieved for a wide variation of the effective interaction. Their conclusion was that the difference between the neutron and proton r.m.s. radii in Pb must be less than 0.2 fm. At higher energies there is more flexibility in the analysis and usually light and self-conjugate nuclei are needed to "calibrate" the effective interaction before applying it to heavier nuclei. The results of Tatischeff *et al.* [2]) for light and medium weight nuclei are in excellent agreement with the present results. In particular, they find $\langle r^2\rangle_n^{\frac{1}{2}} - \langle r^2\rangle_p^{\frac{1}{2}} = -0.07 \pm 0.12$ fm for ^{40}Ca. However, for ^{120}Sn and ^{208}Pb they find the values of 0.23 ± 0.09 fm and 0.25 ± 0.09 fm respectively, somewhat larger than the values obtained in the present work.

An analysis [3]) has been made, in terms of nuclear sizes, of reaction cross sections of π^- mesons on nuclei in the momentum region from 20 to 60 GeV/c. Assuming the neutron and proton distributions in C are identical it is found that for Pb the r.m.s. radii of the two distributions differ by less than 0.1 fm.

An indirect method for the study of neutron distributions is the analysis of Coulomb displacement energies [4]). In this method the r.m.s. radius of the $N-Z$ excess neutrons is determined from the experimental Coulomb displacement energy between an analog state and its parent state and from the experimental value for the r.m.s. radius of the charge distribution in the parent nucleus. The r.m.s. radius of the whole of the neutron distribution can then be determined only if assumptions are made regarding the distribution of the Z core neutrons. The situation is complicated further by the existence of the Nolen and Schiffer [42]) anomaly. It is possible, therefore, that values of $\langle r^2\rangle_n^{\frac{1}{2}}$ derived from analyses of Coulomb displacement energies could be unreliable.

The study of neutron pickup reactions below the Coulomb barrier can lead to direct information on the distribution of the excess neutrons. The values obtained by Korner and Schiffer and by Friedman *et al.* [5]) together with the assumption that the 82 core neutrons in ^{208}Pb have an r.m.s. radius equal to $\langle r^2\rangle_p^{\frac{1}{2}}$ or perhaps 0.1 fm smaller, lead to $\langle r^2\rangle_n^{\frac{1}{2}} - \langle r^2\rangle_p^{\frac{1}{2}} = 0.1$ and 0.2 fm, which is not inconsistent with the conclusions of the present experiment.

We conclude that all other experiments which can provide information on neutron distributions are in agreement with our conclusions for light and medium-weight nuclei. For heavier nuclei our results favour $\langle r^2\rangle_n^{\frac{1}{2}}$ about 0.1 fm smaller than obtained from some other experiments.

7. Conclusions

It has been shown in the present work that the study of the reaction cross sections of π^+ and π^- mesons on nuclei can provide useful information on the density distribution of neutrons. In particular, this information derives mainly from the ratios of the π^--nucleus to π^+-nucleus reaction cross sections and it has been demonstrated that some cancellations of possible errors occur both in the experiment and in the calculations when ratios are studied. The results of the present experiment, when interpreted in terms of neutron distributions, are that in all the nuclei studied (C, Al, Ca, Ni, Sn, Ho and Pb) the neutrons have the same r.m.s. radius as the protons, to within ± 0.1 fm. For ^{40}Ca, the heaviest self-conjugate nucleus, our results favour a value of -0.05 fm for $\langle r^2\rangle_n^{\frac{1}{2}} - \langle r^2\rangle_p^{\frac{1}{2}}$. For light and medium-weight nuclei the present results are in agreement with those obtained from other experiments and from various nuclear matter calculations for finite nuclei. For the heavy nuclei, and in particular Pb, our value for $\langle r^2\rangle_n^{\frac{1}{2}}$ is about 0.1 fm less than the results obtained from some other experiments, and the same applies when comparing the present results with most theories.

The present experiment has also provided interesting information about the pion-nucleus interaction. As far as the calculation of reaction cross sections is concerned, the first order impulse approximation is remarkably successful, provided Fermi-averaged scattering amplitudes are used and also the momentum-transfer dependence of these amplitudes is included. There are interesting, though small, discrepancies at the high and low momentum ends of the range of incident pion momenta we have studied and these call for a more profound examination of pion-nucleus multiple scattering theory. The largest deviations between theory and experiment are about 10 % in the absolute values of σ_R. This general standard of agreement using a theory with no adjustable parameters enhances confidence in the analysis of the ratios σ_R^-/σ_R^+.

We would like to thank Mrs. J. Hilton for her assistance with some of the computer programming and C. A. Baker, A. G. D. Payne, C. J. Reason, F. J. Swales and F. Uridge for their work on the experimental equipment and the running of the experiment. We would also like to thank R. A. J. Riddle, L. H. Watson and J. L. Weil for their assistance in taking the data and J. Cox for his contribution to the early stages of this experiment.

References

1) G. W. Greenlees, G. J. Pyle and Y. C. Tang, Phys. Rev. **171** (1968) 1115;
G. W. Greenlees, W. Makofske and G. J. Pyle, Phys. Rev. **C1** (1970) 1145;
G. W. Greenlees, V. Hnizdo, O. Karban, J. Lowe and W. Makofske, Phys. Rev. **C2** (1970) 1063
2) D. F. Jackson, Phys. Lett. **14** (1964) 118; Nucl. Phys. **A123** (1969) 273;
B. Tatischeff and I. Brissaud, Nucl. Phys. **A155** (1970) 89;
C. J. Batty and E. Friedman, Phys. Lett. **34B** (1971) 7;
C. J. Batty, E. Friedman and D. F. Jackson, Nucl. Phys. **A175** (1971) 1;
A. M. Bernstein and W. A. Seidler, Phys. Lett. **34B** (1971) 569;
B. Tatischeff, I. Brissaud and L. Bimbot, Phys. Rev. **C5** (1972) 234;
I. Brissaud, Y. Le Bornec, B. Tatischeff, L. Bimbot, M. K. Brussel and G. Duhamel, Nucl. Phys. **A191** (1972) 145

3) C. J. Batty and E. Friedman, Nucl. Phys. **A179** (1972) 701
4) See the review article by J. A. Nolen Jr. and J. P. Schiffer, Ann. Rev. Nucl. Sci. **19** (1969) 471
5) H. J. Korner and J. P. Schiffer, Phys. Rev. Lett. **27** (1971) 1457
6) C. J. Batty and G. W. Greenlees, Nucl. Phys. **A133** (1969) 673
7) J. W. Negele, Phys. Rev. **C1** (1970) 1260
8) A. Abashian, R. Cool and J. W. Cronin, Phys. Rev. **104** (1956) 855
9) E. D. Courant, Phys. Rev. **94** (1954) 1081
10) L. R. B. Elton, Nuclear sizes (Oxford, 1961) p. 93
11) E. H. Auerbach, H. M. Qureshi and M. M. Sternheim, Phys. Rev. Lett. **21** (1968) 162
12) M. M. Sternheim and E. H. Auerbach, Phys. Rev. **C4** (1971) 1805
13) G. Charpak, R. Bouclier, T. Bressani, J. Favier and C. Zupancic, Nucl. Instr. **62** (1968) 262
14) K. L. Brown, B. K. Kear, S. K. Howry, Report SLAC-91 (unpublished)
15) R. Meunier, J. P. Stroot, B. Leontic, A. Lundby and P. Duteil, Nucl. Instr. **17** (1962) 20
16) M. Crozon, Ph. Chavanon, A. Courau, Th. Leray, J. L. Narjoux and J. Tocqueville, Nucl. Phys. **64** (1965) 567
17) E. S. Miller, Princeton report PPAD 630F, 1967 (unpublished)
18) R. R. Johnston and K. M. Watson, Nucl. Phys. **28** (1961) 583
19) L. A. Charlton and J. M. Eisenberg, Ann. of Phys. **63** (1971) 286
20) M. L. Goldberger and K. M. Watson, Collision theory (Wiley, New York, 1964)
21) E. H. Auerbach, D. M. Fleming and M. M. Sternheim, Phys. Rev. **162** (1967) 1683
22) G. R. Satchler and R. M. Haybron, Phys. Lett. **11** (1964) 313;
P. G. Roos and N. S. Wall, Phys. Rev. **140** (1965) B1237
23) K. M. Watson, Phys. Rev. **89** (1953) 575;
N. C. Francis and K. M. Watson, Phys. Rev. **92** (1953) 291
24) S. Murugesu, Ph.D. thesis, University of Surrey, 1971
25) A. K. Kerman, H. McManus and R. M. Thaler, Ann. of Phys. **8** (1959) 551
26) T. Lasinski, R. Levi Setti, B. Schwarzschild and P. Ukleja, Nucl. Phys. **B37** (1972) 1
27) R. J. Eden, Rep. Prog. Phys. **34** (1971) 995
28) A. A. Carter *et al.*, Phys. Rev. **168** (1968) 1457
29) G. Höhler and R. Strauss, Tables of pion-nucleon forward amplitudes (University of Karlsruhe, 1970, unpublished)
30) L. L. Foldy and J. D. Walecka, Ann. of Phys. **54** (1969) 447
31) R. J. Glauber, Lectures in theoretical physics, Vol. 1 (Interscience, New York, 1959) p. 315
32) E. Kujawski, Phys. Rev. **C1** (1970) 1651
33) R. C. Johnson and D. C. Martin, Nucl. Phys. **A192** (1972) 496
34) E. H. Auerbach and M. M. Sternheim, Report BNL-12696, 1968 (unpublished)
35) R. J. Glauber, High-energy physics and nuclear structure, ed. G. Alexander (North-Holland, Amsterdam, 1967) p. 311
36) L. R. B. Elton and A. Swift, Nucl. Phys. **A94** (1967) 52
37) S. A. A. Zaidi and S. Darmodjo, Phys. Rev. Lett. **19** (1967) 1446
38) E. Friedman, Nucl. Phys. **A170** (1971) 214
39) D. Vautherin and D. M. Brink, Phys. Lett. **32B** (1970) 149;
J. Zofka and G. Ripka, Nucl. Phys. **A168** (1971) 65;
H. S. Köhler and Y. C. Lin, Nucl. Phys. **A136** (1969) 35
40) B. W. Allardyce *et al.*, Phys. Lett. **41B** (1972) 577
41) D. F. Jackson, Reports on Progress in Physics, 1973, preprint, to be published;
R. C. Barrett and D. F. Jackson, Nuclear sizes and structure, in preparation
42) J. A. Nolen Jr. and J. P. Schiffer, Phys. Lett. **29B** (1969) 396
43) H. R. Collard, L. R. B. Elton and R. Hofstadter, Nuclear radii, ed. H. Schopper, Vol. 2, Group I, Landolt-Bornstein, Numerical data and functional relationships in science and technology (Springer Verlag, Berlin, 1967)
44) J. Friedrich and F. Lenz, Nucl. Phys. **A183** (1972) 523;
R. C. Barrett, Reports on Progress in Physics, 1973, preprint, to be published
45) J. W. Cronin, R. Cool and A. Abashian, Phys. Rev. **107** (1957) 1121
46) F. Binon, P. Duteil, J. P. Garron, J. Gorres, L. Hugon, J. P. Peigneux, C. Schmit, M. Spighel and J. P. Stroot, Nucl. Phys. **B17** (1970) 168